

1 Modelling hourly evapotranspiration in urban environments with 2 SCOPE using open remote sensing and meteorological data

3 Alby Duarte Rocha¹, Stenka Vulova¹, Christiaan van der Tol², Michael Förster¹, Birgit Kleinschmit¹

4 ¹ Geoinformation in Environmental Planning Lab, Technische Universität Berlin, 10623 Berlin, Germany

5 ² University of Twente, Faculty of Geo-Information Science and Earth Observation (ITC), P.O. Box 217, Enschede AE7500,
6 The Netherlands

7 *Correspondence to:* Alby Duarte Rocha (a.duarterocha@tu-berlin.de)

8 **Abstract.** Evapotranspiration (ET) is a fundamental variable to assess water balance and the urban heat island (UHI) effect.
9 Terrestrial ET is deeply dependent on the land cover as it derives mainly from soil evaporation and plant transpiration. The
10 majority of well-known process-based models based on the Penman-Monteith equation focus on the atmospheric interfaces
11 (e.g. radiation, temperature and humidity), lacking explicit input parameters to precisely describe **vegetation and soil**
12 **properties**. The model Soil-Canopy-Observation of Photosynthesis and Energy fluxes (SCOPE) accounts for a broad range of
13 surface-atmosphere interactions to predict ET. However, like most modelling approaches, SCOPE assumes a homogeneous
14 vegetated landscape to estimate ET. **As** urban environments are highly fragmented, **exhibiting a mix of vegetated and**
15 **impervious surfaces, we propose a two-stage modelling approach to capture most of the spatiotemporal variability of ET**
16 **without making the model overly complex**. After predicting ET using the SCOPE model, the bias caused by the assumption
17 of homogeneous vegetation is corrected using the vegetation fraction extracted by footprint modelling. Two urban sites
18 equipped with eddy flux towers presenting different levels of vegetation fraction and imperviousness located in Berlin,
19 Germany, were used as study cases. The correction factor for urban environments has increased model accuracy significantly,
20 reducing the relative bias in ET predictions from 0.74 to 0.001 and 2.20 to -0.13 **for the two sites considering the SCOPE**
21 **model with remote sensing-derived inputs**. Model errors (RMSE) were considerably reduced in both sites, from 0.061 to 0.026
22 and 0.100 to 0.021, while the coefficient of determination (R²) remained similar after correction, 0.82 and 0.47, respectively.
23 **The novelty of this study is to provide hourly ET predictions combining the temporal dynamic of ET in a natural environment**
24 **with the spatially fragmented land cover in urban environments with low computational cost. All model inputs are open data**
25 **available globally for most medium and large cities. This approach can provide ET maps in different temporal resolutions to**
26 **better manage vegetation in cities in order to mitigate the UHI effect and droughts.**

28 **1 Introduction**

29 Evapotranspiration (ET) is essential for understanding the water cycle and energy balance, as it regulates precipitation,
30 temperature and vegetation productivity (Wang et al., 2020; Zheng et al., 2020). The cooling capacity of ET can mitigate the
31 intensity of the urban heat island (UHI), which adversely impacts the health and quality of life of urban residents (Kovats and
32 Hajat, 2008; Scherer et al., 2013). Optimising ET in urban areas could reduce the impact of extreme events such as severe heat
33 waves, drought or flooding (Wang et al., 2020; Ward and Grimmond, 2017). Although ET plays an essential role in planning
34 more sustainable cities, studies in urban environments are rare and very localised due to the challenges of measuring and
35 modelling evaporation from land surfaces to the atmosphere (liquid to vapour): a) evaporation from soil moisture and
36 groundwater; b) evaporation from plant transpiration; and c) evaporation from intercepted precipitation (Miralles et al., 2020;
37 Nouri et al., 2019). The temporal variation of ET is mainly driven by atmospheric conditions such as sunlight intensity (i.e.
38 incoming radiation), air temperature and relative humidity (Foltýnová et al., 2020). In contrast, the quantity of ET is spatially
39 dependent on the vegetation volume and the water availability in the soil (Dwarakish et al., 2015; Wang et al., 2020; Zheng et
40 al., 2020).

41
42 The most suitable system for measuring ET in the urban environment is the eddy covariance (EC) method, which is based on
43 the turbulence flux and energy balance (Liang and Wang, 2020; Nouri et al., 2013). The EC method measures latent heat flux
44 (LE) from the atmosphere using sensors installed over a tower, which can be converted to ET later (Kotthaus and Grimmond,
45 2014). The observations are continually collected over regular time intervals but represented by an irregular area based on
46 footprints that change shape, size and orientation according to atmospheric conditions (Kljun et al., 2015; Kotthaus and
47 Grimmond, 2014). Therefore, EC measurements are affected by atmospheric stability, wind profile and surface roughness in
48 the surroundings of the flux tower (Foltýnová et al., 2020; Schmid and Oke, 1990; Ward and Grimmond, 2017). Soil
49 evaporation, plant transpiration and interception are not separable when measured by this method (Miralles et al., 2020). In
50 addition, anthropogenic sources of latent heat fluxes such as car combustion or air conditioning are undistinguished from the
51 primary sources of terrestrial ET, plant transpiration and soil evaporation (Nouri et al., 2013). Eddy covariance measurements
52 represent a relatively small and constantly varying land cover area around the flux tower (diameter ~500m), insufficient to
53 map ET in a heterogeneous urban environment (Kotthaus and Grimmond, 2014; Nouri et al., 2013; Vitale et al., 2020). Given
54 the high costs to install and operate, it is also impractical to set up a widespread network of flux towers over the city
55 (Westerhoff, 2015).

56 As urban ET observations are rare, costly and available only for a few cities in the world, an alternative is to estimate ET using
57 process-based or empirical models. Fitting classical empirical models or machine learning algorithms are relatively common
58 in natural landscapes but relatively scarce in an urban environment (Vulova et al., 2021; Wang et al., 2020). One reason is the
59 necessity to train the model at representative locations and conditions, which is a challenge in urban areas due to the constantly
60 changing land cover captured by the tower's footprint and lack of flux towers at different surfaces in a highly fragmented and

61 heterogeneous environment (Feigenwinter et al., 2018). In addition, most of the widely used empirical models are unsuitable
62 for variables with strong spatiotemporal dependency, such as ET (Rocha et al., 2018, 2020).

63 The most common types of process-based models to estimate ET (i.e. latent heat flux) are Surface Energy Balance (SEB),
64 hydrological models, Urban Land-Surface Models (ULSM) and Soil-Vegetation-Atmosphere Transfer (SVAT) models. SEB
65 models estimated ET as the residual of the energy balance equation. Some versions, such as Surface Energy Balance Algorithm
66 for Land (SEBAL) and Surface Energy Balance System (SEBS), include variables as land surface temperature, albedo, and
67 net radiation retrieved from remote sensing variables (Nouri et al., 2015; van der Tol and Norberto, 2012). However, SEB
68 models are more suitable for the regional scale and have low performance in the urban environment (Bayat et al., 2018).

69 Hydrological models are **focused** on streamflow, soil moisture storage and runoff generation processes but often also provide
70 estimations of plant transpiration, soil evaporation and interception loss (Devia et al., 2015; Zhao et al., 2013). **Some**
71 **(eco)hydrological models are designed or adapted for urban environments, such as SWMM-UrbanEVA and Urban Climate**
72 **and Hydrology (UT&C), including anthropogenic heating and urban canyon design (Hörschemeyer et al., 2021; Meili et al.,**
73 **2020). However, several parameters are difficult to supply for applications requiring a high temporal and spatial resolution.**
74 **For instance, UT&C requires inputs that are possible only for experimental studies, such as the distance of the wall to a tree**
75 **trunk (m), albedo and emissivity of walls, volumetric heat capacity and thickness for wall and roof layers (Meili et al., 2020).**
76 **Urban Land-Surface Models (ULSM) such as Surface Urban Energy and Water Balance Scheme (SUEWS) and urban climate**
77 **models (UCM) such as PALM-4U are specialised in heat fluxes and microclimates in cities (Järvi et al., 2011; Maronga et al.,**
78 **2015). As most urban models for ET estimation, ULSM models also require several input parameters and a demanding**
79 **calibration process, hampering the model transferability. The accuracy of urban models for LE is often the lowest among all**
80 **fluxes and model outputs, especially in densely built-up areas, undermining their use to estimate ET (Rafael et al., 2020; Ward**
81 **et al., 2016; Ward and Grimmond, 2017).**

82 Soil-Vegetation-Atmosphere Transfer (SVAT) models are based on energy balance and mass transfer, **allowing for a**
83 **comprehensive parameterisation of soil and vegetation surface properties (Kracher et al., 2009; Petropoulos et al., 2009), 2009).**
84 **The Soil-Canopy-Observation of Photosynthesis and Energy fluxes (SCOPE) is a SVAT model that accounts for surface-**
85 **atmosphere interactions of both turbulent heat fluxes and radiative transfer (van der Tol et al., 2009). SCOPE has been**
86 **successfully applied to predict ET in croplands and natural environments (Bayat et al., 2018; Timmermans et al., 2013).**
87 **However, the effect of surface heterogeneity in the horizontal direction is not addressed by (1D) models and SCOPE was never**
88 **applied to urban environments (van der Tol et al., 2009; Yang et al., 2020). The ET estimations from most model approaches**
89 **cited above are based on energy balance and mass transfer methods often derived from the Penman-Monteith equation (Devia**
90 **et al., 2015; Zhao et al., 2013). The Penman-Monteith equations, which are widely used for agricultural applications (Allen et**
91 **al., 2005), focus mainly on the atmospheric interface for a specific vegetation cover. Therefore, most ET modelling approaches**
92 **assume a landscape of homogeneous vegetation without anthropogenic elements to calculate ET from pervious soil and**
93 **vegetation fractions but cannot capture plant phenology (Nouri et al., 2015; Westerhoff, 2015). However, some sophisticated**

94 urban models calculate anthropogenic latent heat flux, the effect of building shadows over vegetated areas and interception
95 loss to provide the total ET (Järvi et al., 2011).

96 Urban environments present highly fragmented and heterogeneous land cover in all dimensions (vertically and horizontally)
97 for both pervious and impervious surfaces (Feigenwinter et al., 2012; Ward and Grimmond, 2017; Zheng et al., 2020). The
98 calibration and processing time to obtain ET in high-temporal and -spatial resolution for large areas for all urban variations is
99 very demanding, if not unfeasible (Zheng et al., 2020). It is also complicated to define a spatial and temporal resolution suitable
100 for most of the required model inputs and outputs (Rafael et al., 2019). For instance, impervious areas are mainly static over
101 a one-year interval, while characterising the weather conditions in an hourly resolution is desirable. Thus, a model that
102 embedded all the interactions between atmospheric conditions, vegetation and soil properties, impervious fractions and
103 anthropogenic heating would be mostly redundant in space or time for hourly ET estimation.

104 This study aims to develop a robust and transferable method to map urban ET at any location in the city using a high-resolution
105 spatiotemporal model that requires only freely available data inputs. The novelty is to provide a solution that combines the
106 high temporal dynamic of ET in a vegetated environment with the spatial fragmentation in urban environments, producing a
107 less computationally expensive but plausible ET product. We assume that terrestrial ET is mostly derived from plant
108 transpiration and soil evaporation, considering these sources to be essential in mitigating the UHI and droughts by better
109 managing green areas in the cities. We neglected interception loss from precipitation and latent heat fluxes from anthropogenic
110 sources such as car combustion or house heating. These sources are not directly associated with ET's cooling effect and may
111 mislead urban planning as they are likely inversely proportional to UHI and droughts. We propose a process-based SVAT
112 model (i.e. SCOPE) combined with a correction factor for urban environments based on vegetation fraction to derive hourly
113 ET. The factor corrects the model bias due to impervious surfaces using vegetation fraction extracted by hourly footprints. The
114 hourly predictions for an entire year (12 months, 24 hours, 8760 timestamps) were compared to reference ET derived from the
115 Penman-Monteith equation and validated with flux tower measurements from two locations in Berlin, Germany. The study
116 focuses on modelling with open data from standard meteorological stations and remote sensing products available for most
117 medium and large cities of Europe, targeting transferability.

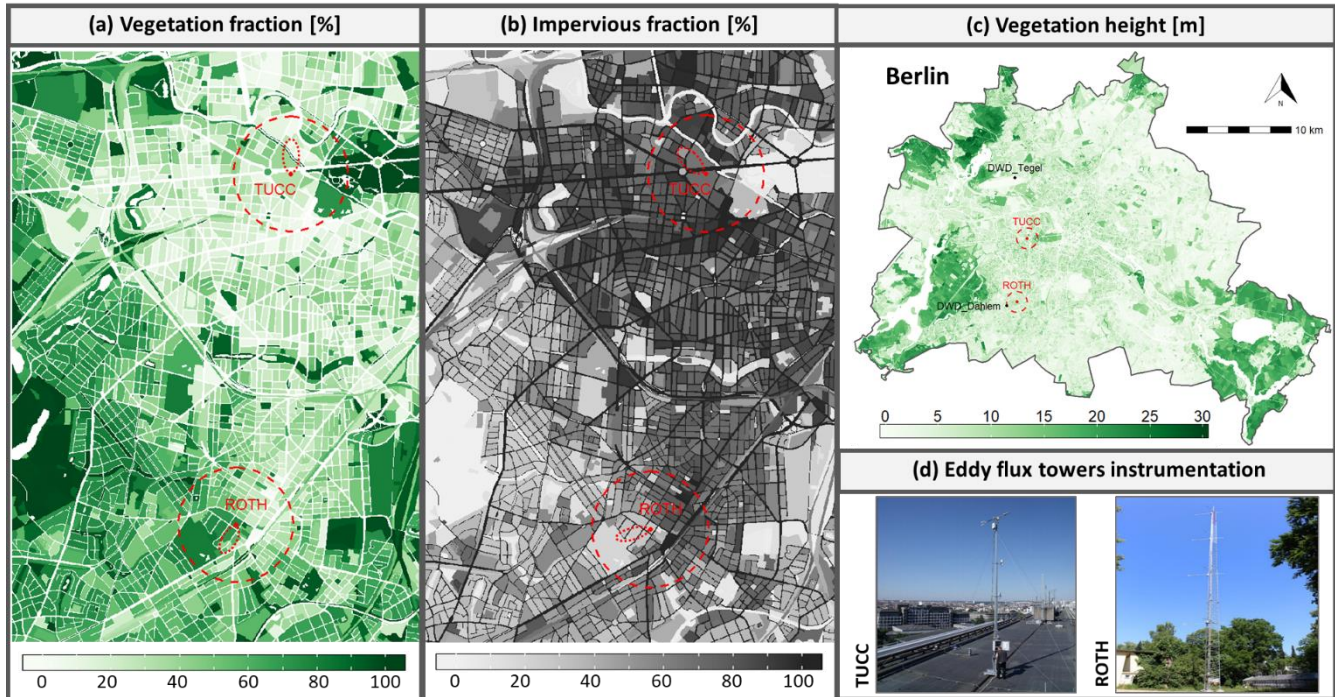
118 **2 Methods**

119 **2.1 Study area**

120 Two sites in Germany's biggest city and capital, Berlin, were selected for this study because they are equipped with eddy flux
121 towers. Berlin is situated in a temperate climate zone with humid sea air, presenting mild temperatures when air masses come
122 from southerly directions and cooler air from the (Atlantic) north (Senate Department for Urban Planning and the Environment,
123 2015). Easterly air masses or continental wind directions usually bring extremely dry air and may cause very cold periods in
124 winter and exceptionally hot days in summer. Berlin is mainly flat with an elevation of 34 meters above the sea (from 24 m to
125 120 m). The maximum annual volume of precipitation occurs in the summer, while winter months present the highest number

126 of hours under rainfall. The lowest precipitation (volume and occurrences) is often in the transitional seasons, with the driest
127 month usually being April (Fig. 2).

128



129

130

131

132

133

134

Figure 1. Locations of the two sites with the respective (a) vegetation fraction (%), (b) impervious fraction (%) and (c) vegetation height (m) in the surroundings of the flux towers (d). The red dotted areas represent a buffer of 1000 m around the towers (red dot), while the red ellipses are examples of hourly footprints. The black dots on the Berlin map (c) refer to the DWD weather stations Tegel and Dahlem. The three land surface maps were extracted from the Berlin Digital Environmental Atlas (Senate Department for Urban Development and Housing, 2017; Senate Department for Urban Planning and the Environment, 2014).

135

136

137

138

139

140

141

142

Despite being equipped with similar eddy covariance instrumentation, the locations present different levels of vegetation cover and imperviousness. Although both sites have a clear urban character, one site is located in a relatively green neighbourhood, while the other is in a central built-up area, with the two sites 6 km apart from each other (Fig. 1a). The flux tower, referred to as Rothenburgstraße (ROTH), is located in a research garden southwest of the city. ROTH observations are measured at approximately 40 meters above the ground, a few meters higher than the tree canopies and the one building nearby. The other flux tower, called TUB Campus Charlottenburg (TUCC), is located on top of the university's main building in the city centre (Fig. 1d). The TUCC measurements are taken from a tower 10 meters above the roof and 56 meters above the ground. With 72 % imperviousness, the TUCC site is a denser built-up area than the ROTH site with 49 % (Fig. 1b).

143 2.2 Data

144 2.2.1 Eddy covariance flux towers

145 The two eddy covariance (EC) flux towers are operated by the Chair of Climatology at the Technische Universität Berlin
146 (TUB) as part of the Urban Climate Observatory (UCO) Berlin (Scherer et al., 2019; Vulova et al., 2021). The EC measurement
147 system is based on an open-path gas analyser and a three-dimensional sonic anemometer-thermometer (IRGASON, Campbell
148 Scientific). The software EddyPro (Version 6.2.1) was used to derive turbulent fluxes of sensible and latent heat by processing
149 the raw data sampled at 20 Hz. The pre-processing of raw data at 30-min intervals was performed as suggested by Vickers and
150 Mahrt (1997), including physical threshold filtering, statistical screening and spikes elimination. The double rotation method
151 was applied by EddyPro for the calculation of a local streamlined coordinate system as determined by the flow statistics over
152 the 30-min averaging period. Furthermore, EC-data were corrected for air density and sonic temperature for humidity, high-
153 and low-frequency spectral corrections (Moncrieff et al., 1997; Webb et al., 1980).

154 The 30-minute values of latent heat flux (LE, W/m^2) under the following conditions were excluded: (1) observations with flag
155 quality higher than one (Foken, 2008); (2) values outside of the thresholds of -100 W/m^2 and 500 W/m^2 ; (3) observations six
156 standard deviations (SD) greater than the average (outliers), and (4) measurements during precipitation or up to 4 hours after
157 rain events. Items one to three were performed using functions from the R package "FREddyPro" (Xenakis, 2016). The wind
158 directions $17^\circ\text{--}35^\circ$ at TUCC and $54^\circ\text{--}72^\circ$ at ROTH are susceptible to distortion due to the mounting setup of the instrument
159 (wind coming from behind the tower). However, as we are using a deterministic model that does not require training and the
160 effect on the model accuracy for ET was insignificant, these observations were preserved. Negative ET values (condensation)
161 were set to zero as annual sums in millimetres will be provided and we are only interested in the amount of water released into
162 the atmosphere by soil evaporation and plant transpiration processes. The entire year of 2019, including winter and nighttime,
163 was selected as there are EC observations simultaneously available for both towers in 2019.

164 The upward latent heat flux (LE, W/m^2) observations were aggregated to hourly resolution and converted to ET by the
165 expression $\text{ET} = \text{LE}/\lambda$, where λ is the latent heat of vaporisation (J kg^{-1}). ET was calculated from LE as a function of air
166 temperature using the "bigleaf" R package (Knauer et al., 2018) in order to use the same procedure for both observed and
167 modelled LE from SCOPE. After pre-processing, from the 8760 timestamps, 43 % of the ROTH and 42 % of the TUCC data
168 were missing. The remaining values of ET, 4993 and 5104 values respectively, were used to assess the model accuracy. To
169 obtain monthly and yearly estimates from the observed ET, gap-filling is required. Given the strong seasonal and diurnal
170 variation of ET, linear interpolation is not recommended. A standard procedure uses the marginal distribution sampling (MDS)
171 gap-filling algorithm, which considers meteorological variables to account for the daily and annual seasonality (Falge et al.,
172 2001; Wutzler et al., 2018). We performed (MDS) gap-filling using the R package "REddyPROC" (Wutzler et al., 2018).
173 Monthly and yearly values of ET from MDS gap-filling will later be compared with the modelled ET predictions.

174 **2.2.2 DWD meteorological data**

175 In order to use model inputs completely independent from the flux towers, data from the meteorological stations of the German
176 Meteorological Service network (DWD Climate Data Center) were selected based on the distance to the flux towers (DWD,
177 2020). **The data from the meteorological stations, Tegel (~5 km from TUCC) and Berlin-Dahlem (~1 km from ROTH), were**
178 **used as model inputs (Table 1).** The variables shortwave and longwave radiation were collected from the Potsdam station to
179 represent both sites. Potsdam station is located in the neighbouring city with the same name, ~19 km and ~23 km from the flux
180 tower sites.

181 **2.2.3 Remote sensing and GIS data**

182 The LAI300m (V1) product generated by the Global Land Service of Copernicus, the Earth Observation program of the
183 European Commission, provides a valuable estimate of an essential biophysical parameter to model ET (Table 1). The
184 Copernicus product provides a grid of LAI values with 300 meters spatial resolution and ten days temporal resolution (Bauer-
185 Marschallinger and Paulik, 2019). The product is based on PROBA-V data and the LAI was estimated by neural network
186 algorithms trained with MODIS and CYCLOPES products. The product was atmospherically corrected, with outlier removal
187 and cloud masking. Smoothing and gap-filling operations were applied based on the land cover type and temporal performance.
188 A time series of 36 LAI maps for 2019 were downloaded and linearly interpolated to match the timestamp of the observed ET.
189 We assumed that in between the 10-days gap, the differences that occurred were relatively minor and irrelevant to this study.
190 **Although the GIS data such as vegetation height and vegetation fraction are fixed for a specific time,** the corresponding **source**
191 **area of the EC flux measurements (e.g. ET or LE) continually varies in shape, size and orientation.** Therefore, areas of influence
192 (footprints) were calculated every hour of 2019 for both towers to capture the spatiotemporal dynamics of the surface
193 properties. The footprint model, according to Kormann and Meixner (2001), was applied using the R package "FREddyPro"
194 (Xenakis, 2016). The input data for footprint modelling were derived from the flux towers measurements, except for the
195 aerodynamic parameter (z_d), roughness length (z_o) and zero-plane displacement (d). **These parameters were** calculated from
196 building and vegetation height by seasons (i.e. winter, summer, and intermediate) to incorporate changes in tree foliage. For
197 further information about how the parameters were calculated, see Kent et al. (2017) and (Quanz, 2018).
198 **The footprints were based on a regular grid of 10 m resolution with an extent (x, y) of 1000 m from the tower locations (fetch**
199 **size). For each grid pixel, the probability that the source area belongs to the flux measurements influence zone was calculated**
200 **for every hour (Schmid and Oke, 1990). These grids of probabilities, excluding pixels outside of 90 % of the footprint**
201 **likelihood, were multiplied to the raster of the surface property (e.g. vegetation height) to extract average values for each**
202 **timestamp of 2019.** Surface properties to characterise the two Berlin sites were derived from a publicly available GIS database.
203 Vegetation fraction (%) and vegetation height (m) was obtained from the Green Volume publication (edition 2017) from the
204 Berlin Digital Environmental Atlas (Senate Department for Urban Development and Housing, 2017). All the layers of GIS
205 maps were converted to a raster with 10 meters resolution and **resampled to the footprint grid of each tower to extract the**

206 average surface properties per timestamp. The raster layers of each land surface were then multiplied by a footprint raster, and
 207 the resulting pixel values were summed to obtain the weighted averages for each site and timestamp.

208

209 **Table 1.** Datasets and data sources used to model ET in this study

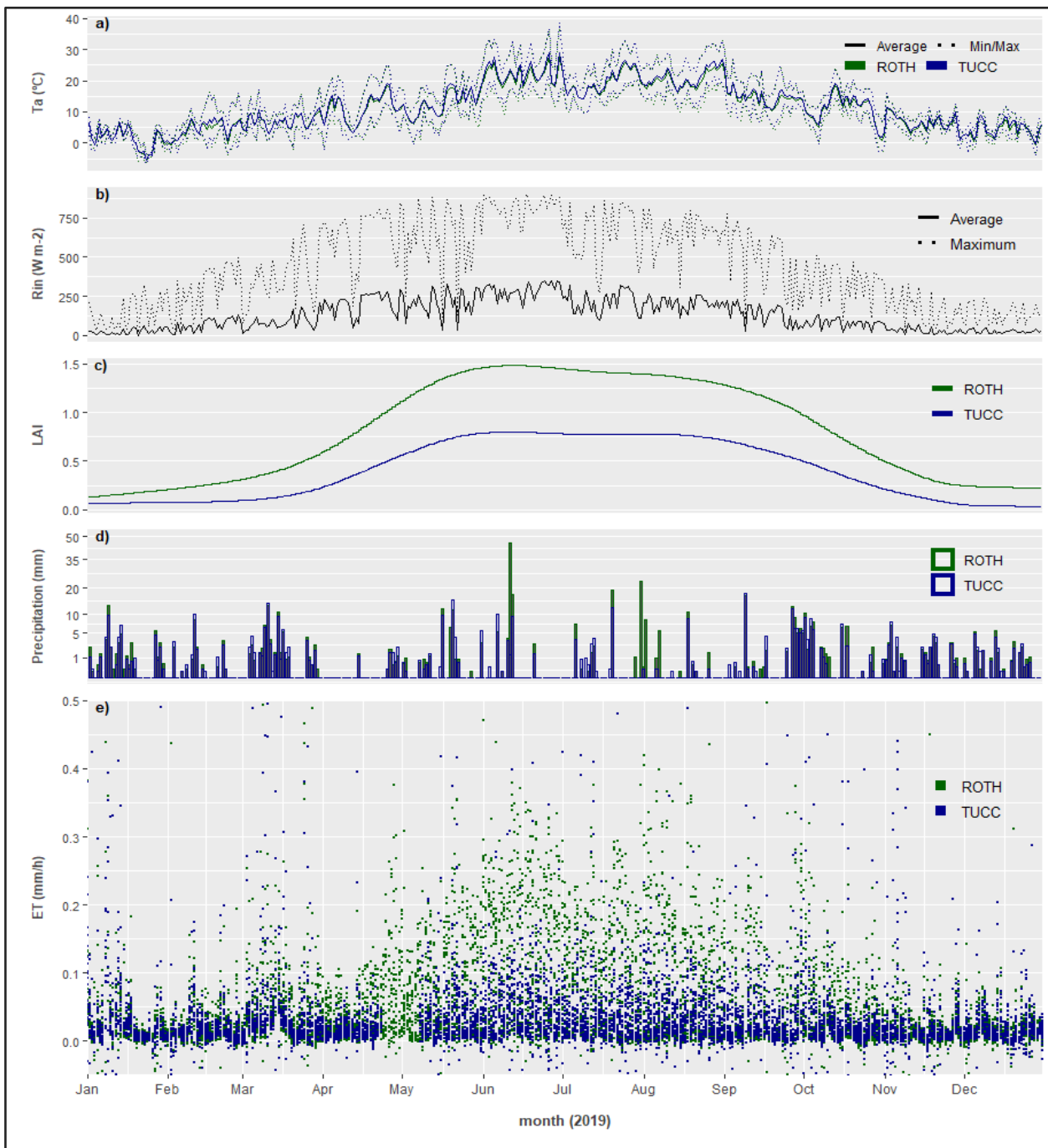
Dataset	Variables	Sources
Meteorological data -DWD stations	Air temperature (T_a , °C), air pressure (p , hPa), relative humidity (rH , %), wind speed (ws , $m\ s^{-1}$) and direction (wd , degree), precipitation events (Oc_prec , yes/no), precipitation volume (V_prec , mm/h), incoming shortwave radiation ^(a) (R_{in} , J/cm^2), incoming longwave radiation ^(a) (R_{li} , J/cm^2).	DWD Climate Data Center http://ftp-cdc.dwd.de/climate_environment/CDC/observations_germany/climate/hourly/
Eddy covariance data - EC flux tower	Latent heat flux (LE , $W\ m^{-2}$), wind speed (ws , $m\ s^{-1}$), wind direction (wd , degree), friction velocity (u^* , $m\ s^{-1}$), Obukhov length (L , m) and northward wind (v_var , $m^2\ s^{-2}$).	Urban Climate Observatory (UCO); Chair of Climatology - Technische Universität Berlin (TUB)
Remote sensing data - Copernicus	Leaf Area Index - 300m resolution (LAI, unitless)	Global Land Service of Copernicus – Portal Distribution http://land.copernicus.vgt.vito.be/PDF/portal/Application.html
RS hyperspectral data - Soil samples	Soil spectral reflectance (Soil_ref, unitless)	It was collected using a field spectrometer (ASD3) with a probe at the ROTH site.
GIS/RS data - Berlin Environmental Atlas, Green Volume (Edition 2017)	Vegetation fraction (Veg_frac , %), vegetation height (hc , m), roughness length ^(b) (z_0 , m) and zero-plane displacement ^(b) (d , m)	Berlin Senate Department for Urban Development and Housing https://fbinter.stadt-berlin.de/fb/wfs/data/senstadt/s_05_09_gruenvol2010

210 (a) R_{in} and R_{li} were later transformed to [$W\ m^{-2}$], and (b) calculated based on the vegetation and building height.

211

212 In this study, water bodies were omitted as they represent only 2.7 % of land cover at the TUCC site and 0 % at ROTH on
 213 average. The Berlin Environmental Atlas also presents a detailed set of maps from the study "Surface runoff, percolation, total
 214 runoff and evaporation from precipitation" (Senate Department for Urban Planning and the Environment, 2019). This study
 215 will be used for comparison with our results.

216



217
 218
 219
 220
 221
 222

Figure 2. Time series of the main variables used in this study for both sites in 2019, where the green colour represents the data from the ROTH site and blue the TUCC site. (a) Air temperature (T_a), the dotted lines represent the maximum and minimum daily values and solid lines represent average daily values; (b) Incoming shortwave radiation (R_{in}) is common for both sites, where the solid black line represents the average and the dotted the maximum daily values; (c) LAI RS-derived values; (d) the volume of precipitation (mm); and (e) the evapotranspiration observations from the EC towers (ET).

223 2.3 Model approaches

224 2.3.1 Penman-Monteith model

225 A formulation based on the Penman-Monteith equation (the ASCE standardised equation for short crops) was used to calculate
226 reference ET (ET_o) (Allen et al., 1998, 2005). Hourly ET_o was calculated by providing air temperature, wind speed, relative
227 humidity, and incoming shortwave radiation as model input using the R package "water" (Olmedo et al., 2016). As this
228 formulation of ET_o assumes a homogeneous landscape of short crops, no land surface information is required, and the model
229 is exclusively driven by meteorological conditions (table 2). Penman-Monteith ET_o is a well-known and established approach
230 which will be used as a benchmarking method to evaluate to what extent including inputs that characterise surface properties
231 can improve ET prediction accuracy.

232 2.3.2 SCOPE model

233 The Soil-Canopy-Observation of Photosynthesis and Energy fluxes (SCOPE) is a process-based model (i.e. SVAT model),
234 which integrates radiative transfer models (RTM) of soil, leaf and canopy with energy balance models (van der Tol et al.,
235 2009). SCOPE is an ensemble model approach, combining one-dimensional bidirectional turbid medium radiative transfer,
236 micrometeorology and plant physiology (van der Tol et al., 2009). This configuration allows SCOPE to account for a wide
237 range of surface-atmosphere interactions, requiring different model inputs according to the target outputs.

238 Since SCOPE is a 1-D vertical model that assumes horizontal homogeneity, it is not designed for heterogeneous urban areas
239 (Yang et al., 2020). However, as our focus is on soil evaporation and plant transpiration, the SCOPE model provides the
240 necessary framework for our application due to the following reasons: (a) the capacity to integrate both high-resolution
241 climatological and medium-resolution remote sensing data inputs for vegetation and soil such as LAI, vegetation height and
242 soil moisture; (b) Sophisticated approach to estimating energy fluxes: SCOPE calculates the essential elements of the energy
243 fluxes, including LE, H, G, net radiation, soil and canopy temperature, friction velocity, and aerodynamic resistance. It also
244 estimates energy fluxes (LE and H) for soil and vegetation separately and warns when the energy balances cannot be closed
245 for a specific timestamp. There are also options to correct for Monin-Obukhov atmospheric stability and V_{cm} for
246 temperature, which is crucial to ET estimation.

247 The model is divided into different modules, allowing the user to focus on essential inputs for estimating heat flux outputs.
248 SCOPE automatically calculates the effect of solar angles on the fraction of sunlit and shaded leaves, reducing the time lag
249 difference between the spectral data and ET observations across the year driven by the fluctuation in sun zenith angle. The
250 calibration and processing time permit high temporal resolution predictions for many different points in space and time. The
251 most important groups of variables to estimate LE are (1) meteorological inputs such as incoming shortwave radiation (R_{in}),
252 air temperature (T_a) and atmospheric vapour pressure (e_a); (2) biochemical plant traits inputs such as the Ball-Berry stomatal
253 conductance parameter (m) and maximum carboxylation capacity (V_{cm}); and (3) biophysical inputs as leaf angle

254 distribution (LIDFa, LIDFb) and LAI (Yang et al., 2020). No anthropogenic heat sources contribute to latent heat fluxes in
 255 SCOPE, nor does building shadow constrain it. Interception loss from precipitation is also not accounted for by the model.
 256 A list of the model inputs that vary across the timestamp used in this study is provided in Table 2. Since changing all model
 257 inputs of SCOPE to realistic values for a time series of hourly observations is almost unfeasible, the other parameters were
 258 kept constant, except for the roughness length (z_0) and zero-plane displacement (d), which were set based on the footprints.
 259 Three scenarios were tested: (1) a SCOPE model with the same input variables as used for reference ETo (Penman-Monteith);
 260 (2) a SCOPE model with all available inputs from the DWD datasets; and (3) a SCOPE model that combines DWD data with
 261 RS data. The model output, total LE (W/m^2), was converted to ET (mm/hour) using the same procedure used for the EC tower
 262 data. The modelling was performed in MATLAB R2018b using SCOPE version 2.0 (Yang et al., 2020).

263 **Table 2.** Input parameters which vary hourly for each SCOPE scenario
 264

Model inputs	SCOPE scenarios		
	ETo	DWD	DWD+RS
Air temperature [$^{\circ}\text{C}$] (T_a)	X	X	X
Relative Humidity [.] (RH)	X	X	X
Wind speed [m s^{-1}] (u)	X	X	X
Incoming shortwave radiation [W m^{-2}] (R_{in})	X	X	X
Incoming longwave radiation [W m^{-2}] (R_{li})		X	X
Air pressure [hpa] (p)		X	X
Solar zenith angle [deg] (tts)		X	X
Leaf Area Index [.] (LAI)			X
Vegetation height [m] (h_c)			X
Soil reflectance [.] ($soil_refl$)			X

265 (tts) was derived from the DWD timestamp. The setting options' soil heat method' and 'applTcorr' to correct v_{cmax} parameter by temperature
 266 were used to run the model scenarios DWD and RS.

267 2.3.3 Correction factor for urban environments

268 Our focus is on the primary sources of terrestrial ET (plant transpiration and soil evaporation). Climatological conditions are
 269 the main drivers of terrestrial ET, which present a high temporal dynamic. On the other hand, fragmented urban land cover
 270 and impervious surfaces are the main constraints of ET released into the atmosphere. Therefore, a model to predict urban ET

271 accurately requires high-temporal and -spatial resolutions. Still, processing all time-space interactions is demanding and
272 currently unfeasible for the resolution needed for our application. However, ET predictions from SCOPE are likely to be biased
273 if the imperviousness areas are not accounted for, as the models assume homogeneous vegetation (horizontally). Based on
274 these assumptions, we propose this two-stage modelling approach to capture most of the spatiotemporal variability of ET
275 without making the model overly complex. First, we predicted ET using the SCOPE model for the described scenarios. Then,
276 we corrected the predictions to represent only vegetated areas extracted from the footprints of each timestamp.
277 This strategy combines hourly SCOPE predictions with high spatial resolution vegetation fraction maps to correct the
278 assumption of homogeneous vegetation and impervious areas. Impervious areas are mainly static over a one-year interval;
279 therefore, embedding urban features and anthropogenic heat sources in the model would be predominantly redundant and very
280 computationally demanding. This approach allows us to predict ET for different spatial and temporal resolutions, which would
281 be more complicated if using a more specialised urban model for hourly ET predictions. In order to correct the ET predictions
282 according to the surface characteristics of each site, we use the extracted vegetation fraction average from the footprints per
283 timestamp to subtract the ET estimated in impervious areas with a 10 meters resolution product.
284 The correction factor for urban environments is a relative value that varies from 0 to 1, where zero means completely
285 impervious and one fully vegetated. The factor is multiplied by the total ET predictions from SCOPE and ETo from Penman-
286 Monteith to provide the corrected estimate for each timestamp. This approach assumes zero ET coming from impervious
287 fractions. However, none of the footprint estimations of the correction factor (i.e. vegetation fraction) was entirely impervious.
288 The ROTH site presents an annual average (footprint) of vegetation fraction of 0.55 (0.15-0.77) and canopy height of 7.7 m
289 (2.9-10.0), while the TUCC site presents an average of 0.27 (0.03-0.87) and 7.1 m (2.7-15.1), respectively. Street trees were
290 considered for the calculation of vegetation height and fraction.

291 **2.3.4 Model assessment**

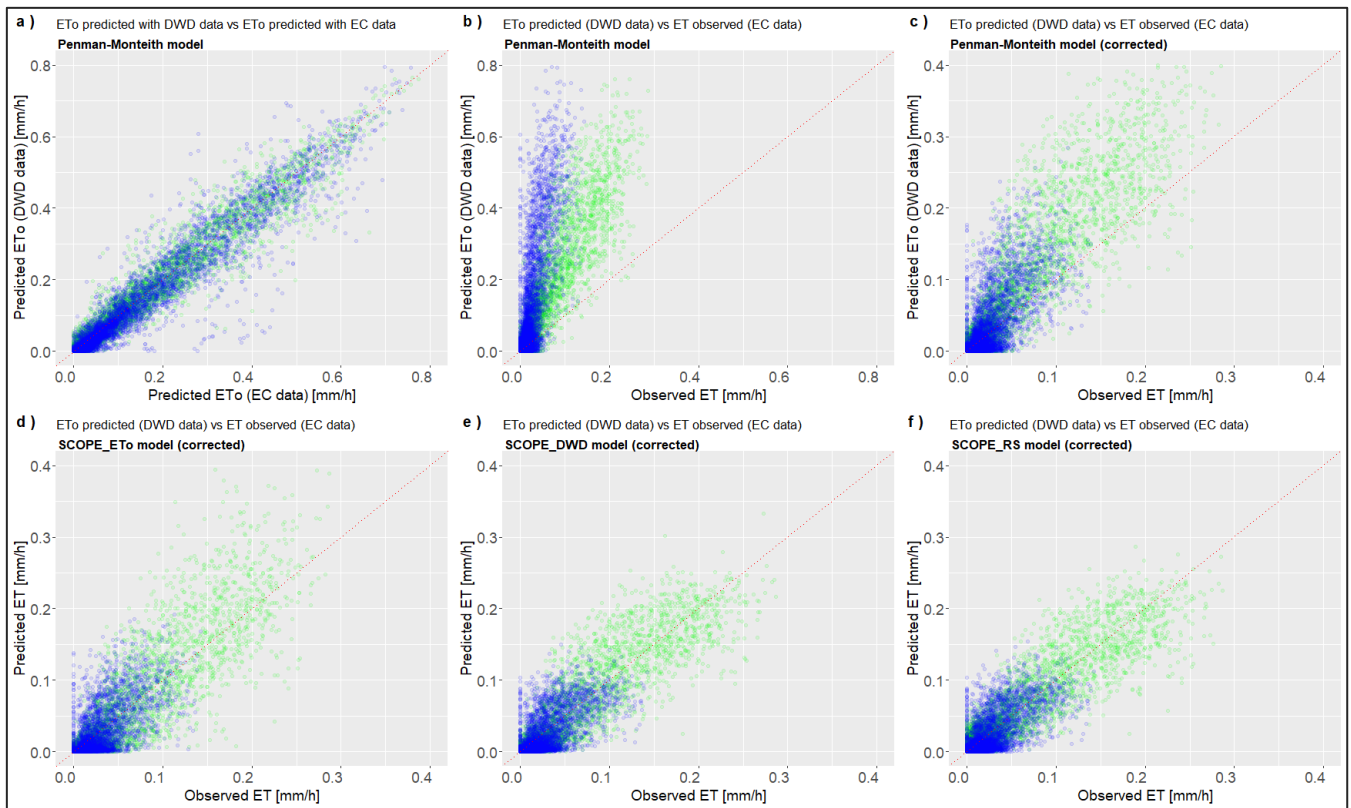
292 As both models are fully deterministic, no train and test splitting or cross-validation approaches are needed to select and
293 validate the models. The model accuracy was assessed using all available ET values from the flux tower time series. To assess
294 model precision, the metrics Root Mean Square Error (RMSE) and the coefficient of determination (R^2) between predicted
295 and observed ET were used. Since deterministic or process-based models are more prone to prediction biases than fitted
296 empirical models, the relative bias (rBias) was assessed. In this study, bias relative to the observed ET was also used as an
297 indicator of the correction factor efficiency in providing unbiased predictions in an urban environment. All plots and metrics
298 for model assessment were performed using the "ggplot2" package (Wickham, 2016) and basic functions in R software (R
299 Core Team, 2020).

300 3. Results

301 3.1 ET prediction in urban environments

302 As atmospheric conditions are the main drivers for evapotranspiration, we first tested the similarity of the climatological
303 variables measured by the flux towers compared to nearby standard meteorological (DWD) stations. The results (Fig. 3a) show
304 that there is a strong relationship between the ETo calculated using data from flux towers (x-axis) and data from DWD stations
305 (y-axis), but also between the locations using the same data. For any of the six combinations of ETo pairs, the coefficient of
306 correlation is at least 0.96 (not shown). This result indicates that a nearby meteorological station can represent the local
307 atmospheric conditions without losing significant accuracy. Therefore, we use only publicly available meteorological model
308 inputs to predict ET, completely independent from the measurements of the two towers. As meteorological variables and
309 vegetation fractions are available for most medium and large cities of Europe, there is a great potential for the methodology to
310 be transferred to other locations based on the promising results shown for the two EC towers in Berlin.

311



312 **Figure 3.** The relationship between ETo calculated using data from the meteorological stations and EC towers data (a), ETo from the DWD
313 data versus observed ET from the EC tower (b), ETo (corrected) versus observed ET (c), corrected SCOPE_ETo inputs versus observed ET
314 (d), corrected SCOPE_DWD versus observed ET (e), and corrected SCOPE_RS versus observed ET (e). The green dots represent the ROTH
315 site, and the blue dots represent the TUCC site.

317 Although atmospheric conditions and water availability mainly drive the temporal variability of ET, the spatial variability,
 318 which determines the volume of ET, depends primarily on the land surface characteristics. The models clearly overestimate
 319 ET in highly fragmented landscapes with impervious surfaces, as shown in Figure 3b. The difference between the two towers
 320 emphasises the dependence on the vegetation fraction. The ROTH site contains a higher average of vegetation and pervious
 321 fractions (55 % and 49 %) than the TUCC site (27 % and 28 %). Therefore, the model bias at ROTH is more than twice as low
 322 as when the model is applied at TUCC without the correction factor (Table 3). As presented before, the ETo of the two towers
 323 is very similar, while the observed ET is twice as low at TUCC.

324 **Table 3.** Model accuracy for each scenario according to the metrics RMSE, R^2 and relative bias for ETo (Penman-Monteith) and SCOPE,
 325 with and without the correction factor for urban environments. The highlighted bold values represent the highest precision and lowest bias
 326 based on each metric.

Model approaches	Input scenarios	Correction for urban environments	ROTH			TUCC		
			RMSE	R^2	rBias	RMSE	R^2	rBias
ETo	ETo	uncorrected	0.126	0.80	1.57	0.165	0.53	3.83
	ETo	corrected	0.051	0.82	0.48	0.033	0.48	0.32
SCOPE	ETo	uncorrected	0.081	0.77	0.71	0.114	0.49	2.22
	ETo	corrected	0.033	0.78	-0.007	0.024	0.45	-0.12
	DWD	uncorrected	0.063	0.82	0.64	0.099	0.51	2.09
	DWD	corrected	0.026	0.83	0.05	0.021	0.47	-0.16
	DWD+RS	uncorrected	0.061	0.81	0.74	0.100	0.51	2.20
	DWD+RS	corrected	0.026	0.82	0.001	0.021	0.47	-0.13

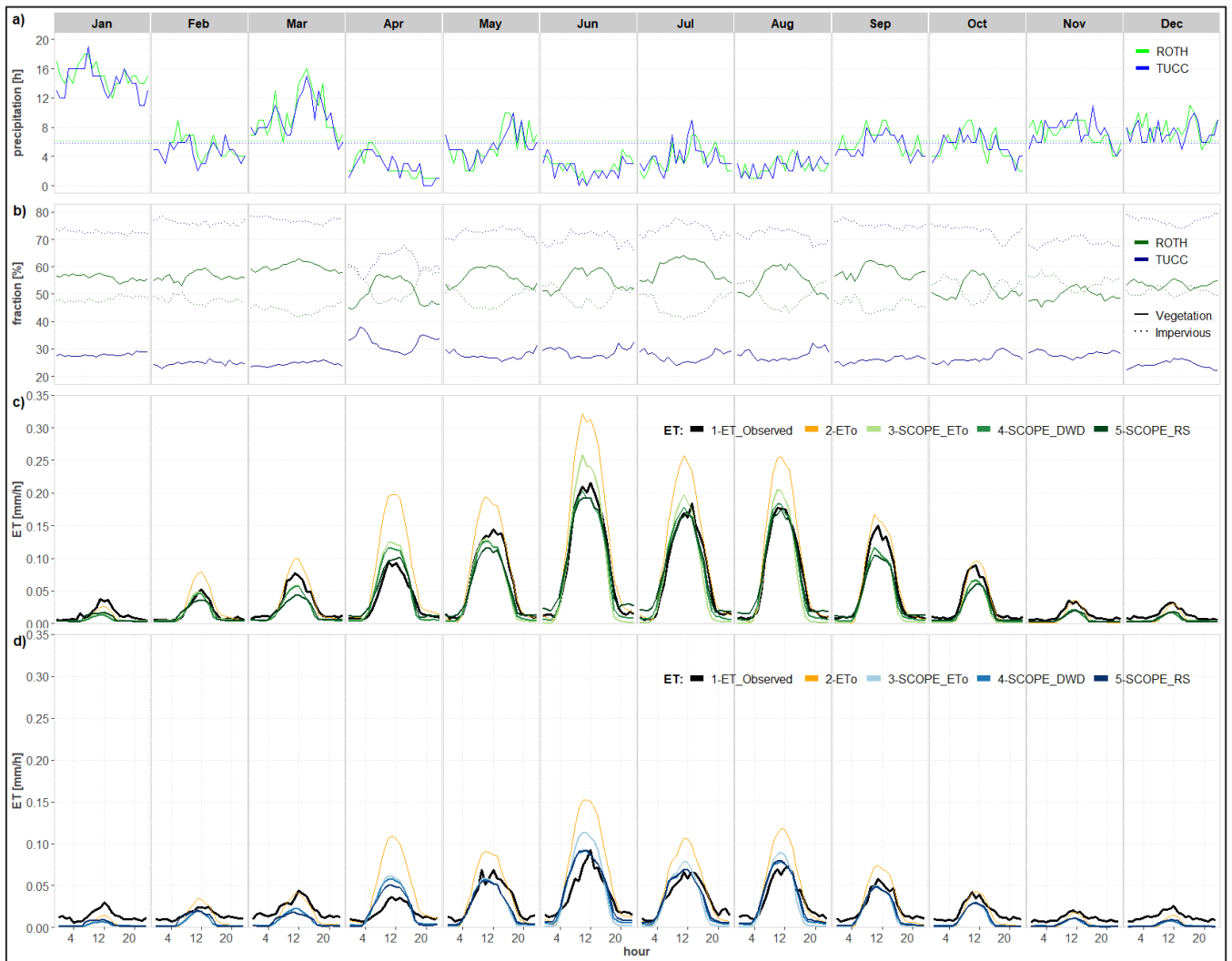
327
 328 The proposed correction factor for urban environments reduces the prediction biases (rBias) and model errors (RMSE)
 329 significantly. The corrected ETo prediction from Penman-Monteith, which initially presents a rBias of 1.57 and 3.83 (ROTH
 330 and TUCC), is reduced to 0.48 and 0.32, respectively (Table 3). For ROTH, while RMSE has decreased by a factor of more
 331 than two after the predictions were corrected, the R^2 value was kept similar to the original. For TUCC, RMSE was reduced
 332 even further, but also the R^2 , which was caused by a reduction in the range of values after being corrected. Despite the
 333 significant improvement using the correction factor, ET prediction based on ETo is still biased, which agrees with other authors
 334 that have reported recurrent overestimation from Penman-Monteith models even at fully vegetated areas (Allen et al., 2005;
 335 Ortega-Farias et al., 2004).

336 SCOPE model outputs have similar R^2 but drastically reduce the relative bias and model error for the corrected predictions
337 compared to ETo predictions. The SCOPE model using the same input variables as the ETo model is more accurate than the
338 Penman-Monteith model. However, the model accuracy is further improved (R^2 of 0.82 and RMSE of 0.026) by the inclusion
339 of other DWD scenario input parameters such as incoming longwave radiation (Rli) and atmospheric pressure (p). The SCOPE
340 models for the RS and DWD scenarios for ROTH present a similar accuracy but lower bias, 0.1 % (RS) against 5 % (DWD).
341 The reduction in bias in the RS scenario can be explained by the inclusion of LAI, which provides a more precise estimation
342 of the vegetation structure in the early season, improving the ET predictions considerably for April. **The SCOPE_RS model**
343 **for TUCC presents an even smaller RMSE (0.021) but a much smaller R^2 and higher bias than ROTH.** The ET range partially
344 explains these differences in R^2 between the two towers, varying from 0 to 0.29 mm at ROTH and from 0 to 0.16 mm at TUCC.

345 **3.2 ET seasonality**

346 ET varies greatly across the day and seasons according to changes in meteorological conditions (e.g. temperature, radiation),
347 plant phenology (e.g. LAI, stomatal conductance) and water availability (dry and wet seasons). Figure 4 (c) and (d) shows the
348 variability in average hourly ET across the months between the two towers (black line). The differences in scale between the
349 two sites are clear, but they present very similar behaviour across time. The predictions using corrected ETo (orange line)
350 overestimate ET from February to October for ROTH and from April to September for TUCC but fit well otherwise. The
351 corrected SCOPE models exhibit the opposite behaviour, being more accurate around the spring-summer and **underestimating**
352 otherwise.

353 **Observed ET is only higher than predicted ETo in January and December for both sites.** The periods when SCOPE models
354 underestimate predictions correspond precisely with the months in which the number of hours of precipitation is higher than
355 the average (Fig. 4a). April was an extremely dry month, and all models overestimated ET for both sites, as ET is limited by
356 underground water. A second condition occurred in April, causing a significant increase in vegetation fraction and a decrease
357 in impervious fraction extracted from the footprints at the TUCC site. Atmospheric conditions have led to overall greener
358 footprints as they were atypically concentrated in a vegetated area (park), reducing the effect of the correction factor without
359 increasing ET values. This phenomenon may occur at TUCC because the tower is located on the top of a building completely
360 sealed with a surrounding wall (Fig. 1) and the effect of dry and wet surfaces are more noticeable there than at ROTH.

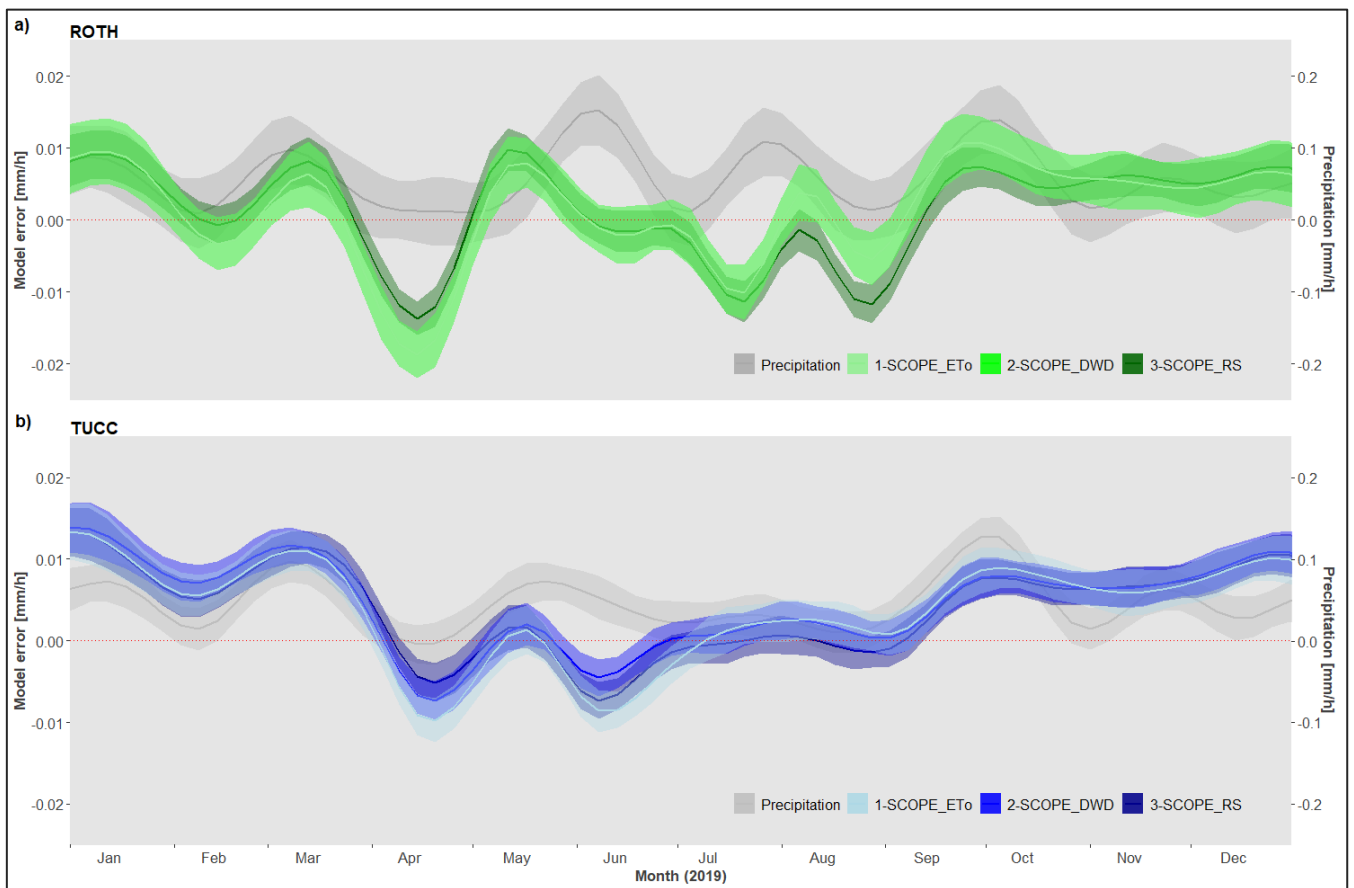


361
 362 **Figure 4.** Hourly averages per month in 2019 for (a) precipitation events; (b) percentage of vegetation fraction (solid line) and impervious
 363 fraction (dashed lines); (c) predictions for the ROTH site; and (d) predictions for the TUCC site. The observed ET (black line) and corrected
 364 ETo (orange line) for both sites. The corrected SCOPE predictions are represented by green lines for ROTH and blues for the TUCC site.
 365 The light to dark colours represent SCOPE_ETo, SCOPE_DWD and SCOPE_RS, respectively, for both sites.

366

367 **Analysing model accuracy in the time series, as expected, the error (mm/h) is not randomly distributed around zero across the**
 368 **year.** The predictions, in general, are overestimated in summer and underestimated in winter. **As both approaches are**
 369 **deterministic, there is no assumption of the independent and identical distribution residuals as in empirical models.** However,
 370 **temporal distribution in the residuals (autocorrelation)** can help identify in which **environmental** conditions the precision and
 371 bias in predictions affect the overall accuracy. In our case, Figure 5 clearly shows that model bias is strongly related to the
 372 volume of rain over the season.

373



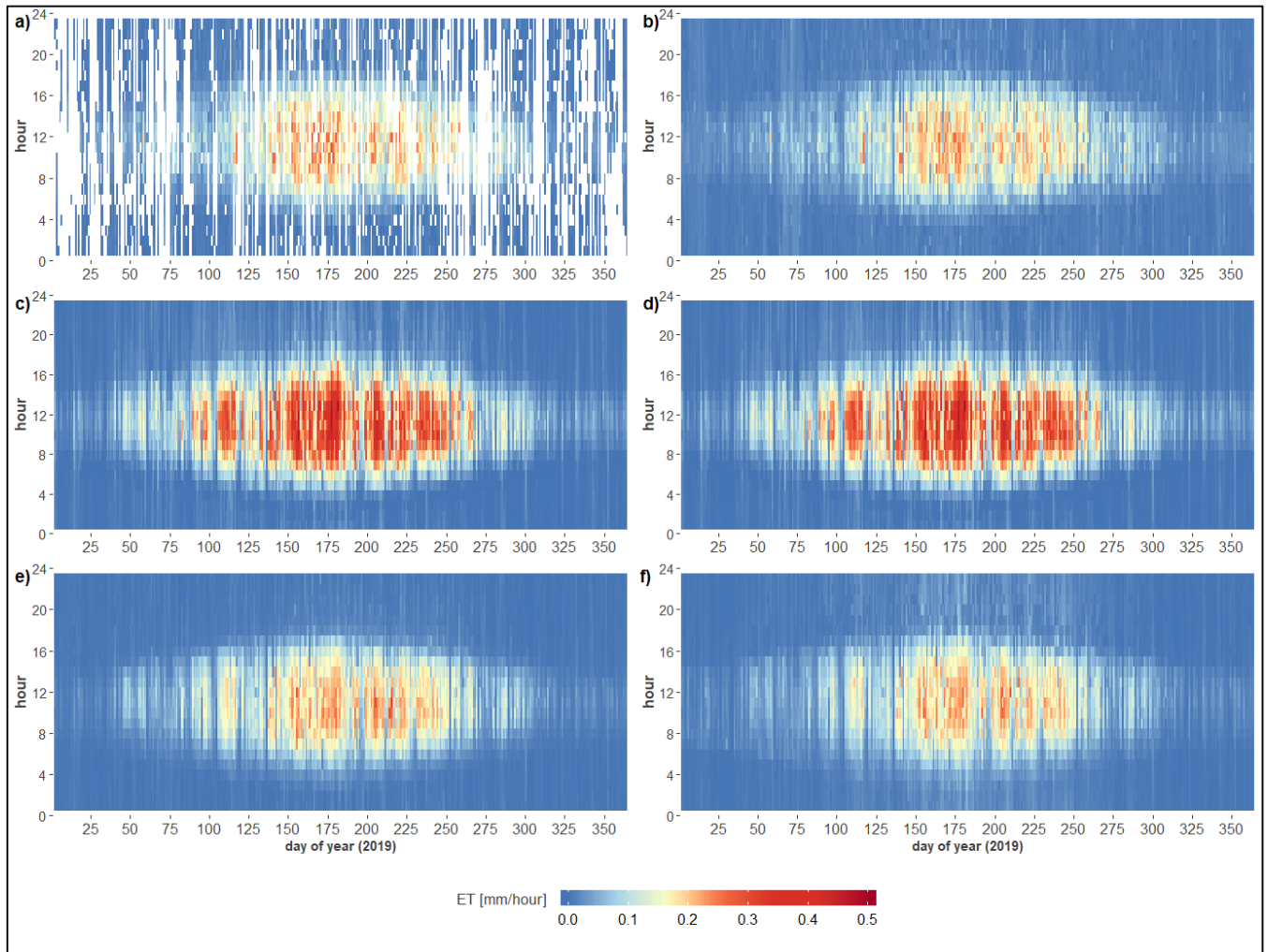
374 **Figure 5.** Smoothed time series of the volume (mm/h) of precipitation (grey line) and model error (observed-predicted) for the ROTH site
 375 (a) and the TUCC site (b). Smoothing function (formula = $y \sim \text{splines}::\text{bs}(x, 20)$).
 376

377 The curve of the SCOPE model errors has very similar behaviour compared with the millimetres of rainfall across the year.
 378 When the volume of precipitation is over a certain threshold (around 0.5 mm/h), the ET predictions are underestimated, while
 379 the model often overestimates ET below the threshold. The predictions based on ETo are most overestimated during the spring
 380 and summer seasons. The year 2019 was extremely dry, Germany's third-warmest year since 1881 (German Weather Service
 381 - DWD), partially explaining the overestimated ET values, especially in the most vegetated site (ROTH, Fig. 5b).

382 3.3 Monthly and yearly ET estimations

383 As 42 % of the hourly ET observations were missing values, we performed the MDS gap-filling method to estimate monthly
 384 or yearly observed ET values. 336 mm/year was estimated for the ROTH site, representing 66 % of the observed annual
 385 precipitation (Fig 6). This value is similar to the corrected SCOPE RS model, 330 mm/year or 65 % of the annual precipitation
 386 according to the nearby DWD meteorological station. The corrected ETo annual estimate of 477 mm/year (94 %) is most likely
 387 overestimated. At the TUCC site, MDS gap-filling estimates 188 mm/year, representing nearly half of the annual precipitation
 388 volume (47 %), which is much lower than at ROTH. The ETo estimated at TUCC is 236 mm, representing 59 % of the annual

389 precipitation, while the SCOPE models estimate the lowest values, ranging from 146 to 151 mm/year (36 % to 38 %). The
390 maximum volume of precipitation for ROTH (i.e. Dahlem station) was observed in June (75 mm) and the minimum in April
391 (6 mm). The maximum value of estimated ET was 95 mm for ETo and 67 mm for SCOPE_RS, also in June, while the minimum
392 was 6 mm and 4 mm respectively in January. The TUCC site (i.e. Tegel station) presents a maximum volume of precipitation
393 in March (62 mm) and the minimum also in April (7.5 mm). The ET estimate reaches the maximum of 49 mm and 32 mm for
394 ETo and SCOPE_RS models in June and a minimum of 3.2 mm and 2.2 mm in December, respectively.
395



396
397 **Figure 6.** ET by day of the year and hours of the day for the ROTH site. Observed ET after cleaning (a), observed ET gap-filled with MDS
398 (b), Penman-Monteith ETo (c), predicted ET with SCOPE_DWD model (d), predicted ET with SCOPE_ETo model (e), and predicted ET
399 with SCOPE_RS model (f). For TUCC, see Fig. A1 in Appendix A.

400 4. Discussion

401 4.1 Urban environment and ET

402 As demonstrated in this study, the approach combining a correction factor for urban environments with a SVAT model can
403 provide accurate predictions of ET, similar to the values measured by the eddy covariance method. However, our approach
404 offers a low-cost and less computationally intensive method to estimate ET using data from standard meteorological stations
405 combined with freely available remote sensing data. The reduced number of model inputs optimises calibration time, and
406 parsimony often results in more transferability. Data from stations provide consistent measurements with nearly no missing
407 values, while EC data often present significant gaps. We also showed that similar atmospheric conditions would produce very
408 distinctive ET values as the process is highly dependent on the vegetation fraction of the location under consideration. As a
409 sum of evaporation from the soil, plant transpiration and intercepted precipitation, the volume of water released into the
410 atmosphere by ET varies significantly according to the imperviousness. Our assumption that most terrestrial ET could be
411 attributed to the two primary processes of soil evaporation and plant transpiration seem to be valid for the urban environment.
412 The most vegetated urban site (ROTH) has presented a high accuracy for the ET predictions and no bias after the proposed
413 correction. Furthermore, daytime ET in the summertime is twice as high in ROTH, the highly vegetated site, as in TUCC,
414 demonstrating the dominant contribution of transpiration to urban ET.

415 Despite the predominant role of soil evaporation and plant transpiration, interception loss is also a substantial component of
416 urban ET. According to Ramamurthy and Bou-Zeid (2014), wet impervious surfaces evaporate at higher rates than wet
417 vegetation as they often store more heat. They conclude that evaporation from wet impervious surfaces such as concrete
418 pavements, asphalt and building rooftops accounted for around 18 % of the LE and may last up to ten days, with the highest
419 evaporation rates occurring 48 hours after a precipitation event. The EC tower at the TUCC site is installed 10 m over a building
420 with a flat roof, intensifying the interception loss even in low radiation and air temperature conditions. For the denser built-up
421 site (TUCC), the lower accuracy and the relative underestimation (-0.13 of bias) in comparison to ROTH could mostly be
422 attributed to interception loss combined with higher land surface temperature caused by anthropogenic heating (Fig. 5b). Based
423 on Figs. 4 and 5, the interception loss could explain most of the model error at the TUCC site, indicating that the impervious
424 urban canopy may intercept more precipitation and evaporate faster than the vegetated canopy.

425 The monthly and annual ET values may be underestimated, especially in the highest built-up areas, as interception loss and
426 precipitation are not part of the model. Furthermore, in winter, condensation generates wet surfaces at night (cars, windows,
427 roads, metal roofs), which evaporate again during the day, increasing the ET measured by the EC method, similarly to
428 interception loss. The model underestimation occurs mainly at night and winter, which makes us conclude that direct
429 anthropogenic heat sources have a minor contribution to LE during the spring and summer. However, during winter, neither
430 moisture nor the cooling effect capacity of ET is important in this part of the globe.

431 The intercepted precipitation on impervious surfaces does play a role in increasing the evaporation after rainfall, as
432 demonstrated by the underestimated model prediction in the period when more frequent rain events occur (Fig. 5). However,

433 intercepted precipitation is an independent process that should not be mixed with evaporation from plants and soil for two
434 reasons. First of all, it is difficult to assess the contribution of interception loss to measured LE, as the EC data during and just
435 after rain is not available (missing values) or non-reliable. Wouters et al. (2015) could only select four events with at least 18
436 continuous hours observed after rainfall due to data gaps during these periods. The authors conclude that ET increases
437 immediately after rain in the daytime and remains high up to 12 hours, estimating that 12.5% of the precipitation evaporates
438 from impervious surfaces at one of the sites. The second reason is that despite increasing ET and affecting the EC
439 measurements, interception loss from impervious surfaces does not mitigate UHI, droughts or make cities more sustainable.
440 On the contrary, partially- or non-sealed surfaces favour percolation, recharging the groundwater and maintaining soil moisture
441 (Gillefalk et al., 2021). Also, depending on the topography, the capacity to store water on impervious surfaces can vary greatly.
442 Classical process-based models using the Penman-Monteith equation focus mostly on the atmospheric interfaces, lacking
443 representation of soil and vegetation properties. The crop or grassland factors suggested for the Penman-Monteith equation are
444 often calibrated for the growing season in optimal conditions (Allen et al., 1998), which otherwise overestimate ET. However,
445 using variables to characterise plant phenology and water availability in the soil offered in the SCOPE model allows for a
446 comprehensive parameterisation to capture the ET variation in the vegetated areas of the city (van der Tol et al., 2009). The
447 effect of surface heterogeneity in the horizontal direction, typical in an urban environment, is not addressed by (1D) SCOPE
448 or Penman-Monteith-based models. However, accounting for surface-atmosphere interactions in vegetated fractions with a
449 SCOPE model combined with high-resolution land cover to mask the impervious areas makes it possible to predict ET
450 accurately in urban environments.

451 **4.2 ET time series and model validation**

452 The EC system used in this study is one of the most suitable approaches for deriving observed terrestrial ET, especially in
453 urban areas (Foltýnová et al., 2020; Nouri et al., 2013). Nevertheless, there are some drawbacks to EC measurements, such as
454 (1) LE is a measurement of energy to transform water to vapour (ET) but also the other way around (condensation), which
455 produces negative ET values; (2) The source area representing EC measurements varies continuously in size and shape, which
456 make difficult to identify the surface from which ET is released in heterogeneous urban environments (Kljun et al., 2002;
457 Kotthaus and Grimmond, 2014; Schmid and Oke, 1990); (3) During rain and after a certain subsequent period, EC
458 measurements are not reliable, presenting unrealistically high values of ET (Kotthaus and Grimmond, 2014; Ward et al.,
459 2013a); (4) Anthropogenic vapour emissions such as car exhaust or building heating are accounted as ET as well (Karsisto et
460 al., 2016; Kotthaus and Grimmond, 2012; Nordbo et al., 2012; Ward et al., 2013a); and (5) It is not possible to separate
461 evaporation into soil evaporation, plant transpiration and interception loss from precipitation (Nouri et al., 2013).

462 Despite the EC method being the closest attempt to measure ET directly, studies have reported accuracy varying from 5 % to
463 20 % (Foken, 2008; Liang and Wang, 2020), which may be even higher in urban environments as the lack of energy balance
464 closure is more pronounced. The ET concept also raises open questions about whether terrestrial ET should be considered zero
465 during rain or nighttime and to what extent all mentioned evaporation processes exhibit similar seasonality. For instance, soil

466 evaporation and plant transpiration are strongly correlated (in energy-limited regions) as they have similar drivers. On the
467 other hand, vaporisation of intercepted water behaves differently across seasons, and it is mainly driven by precipitation and
468 less constrained by net radiation (Webb et al., 1980). However, interception can exceed daytime transpiration rates even at
469 night and is disproportionately high in winter (Martens et al., 2017; Miralles et al., 2020). A combination of sap flow and flux
470 tower measurements could increase the understanding of under what circumstances or atmospheric conditions (in particular
471 solar radiation and precipitation) ET measurements based on eddy covariance agree with the water uptake by trees.
472 The differences between evaporation processes also vary across space in an urban environment and present space-time
473 interactions. For instance, the ROTH site presents a considerably higher overall ET and vegetation fraction, but the average
474 ET at night at TUCC is higher than at ROTH for all seasons. ET shows a moderate correlation (0.35 and -0.44) with vegetation
475 fraction and impervious fraction extracted from the footprints for the ROTH site but no significant correlation for the TUCC
476 site. However, vegetation fractions can partially explain the difference between observed ET and reference ET (ET_o) in spring
477 and summertime, presenting a correlation of 0.44 for the TUCC site and 0.62 when both locations are analysed together. In
478 summer at the ROTH site, the percentage of vegetation fraction increases during the day up to noon, while the impervious
479 fraction presents the opposite behaviour (Fig. 4b), which may partially explain the better correlation. These differences in
480 footprint size across the day are affected by alterations in atmospheric stability and wind speed, which, combined with the
481 vegetation-impervious composition in the tower surroundings, determine the vegetation fraction in the zone of influence.
482 The discrepancy between the concept of modelled ET and the direct EC measurements makes model validation challenging.
483 Some of the model bias could be attributed to the flux tower measurements. For instance, the underestimation in the ET
484 predictions around winter and periods with higher precipitation could be an artefact of bias in EC measurements caused by
485 water in the instrument. Ward et al. (2013) also indicate that LE measured by the EC method presents significantly higher
486 values than modelled LE in the following hours after rainfall. EC measurements can also be unreliable during certain conditions
487 such as non-steady-state or absence of well-developed turbulence. LE measurements from EC towers are reported as slightly
488 underestimated due to the lack of closure in energy balance caused by low turbulence (Kracher et al., 2009).
489 Both predictions and observations present a certain level of bias and imprecision (random and systematic errors) that behave
490 differently according to the environmental conditions and model calibration. Therefore, when seeking global model accuracy,
491 one may increase the bias to fit the observed ET better in general, affecting predictions in other conditions in which the model
492 could be closer to reality than the EC measurement. A better approach would be to calibrate the model separately for different
493 conditions. For instance, the bias values for TUCC can be further reduced if the correction is applied only during the daytime
494 or if LE soil and LE canopy estimates from the SCOPE model are corrected by vegetation fraction and impervious fraction
495 separately (not shown). Also, model accuracy was significantly improved when the option to correct the parameter v_{cmax} by
496 the hourly temperature was selected, showing that the seasonality of photosynthetic parameters is highly important for ET
497 estimates.
498 The inclusion of remote sensing data proved beneficial in modelling urban ET using SCOPE. Important plant phenology
499 parameters such as LAI, water content and chlorophyll (Chl) can be obtained using available satellite images (Raj et al., 2020).

500 Our study included remote sensing-derived LAI from Copernicus, reducing bias in ET predictions in the early spring.
501 Incorporating LAI was particularly beneficial in April, as using the default constant value of LAI overestimates ET. In 2019,
502 the air temperature started to increase in this period, but the canopy foliage was still incomplete. The inclusion of canopy
503 height in combination with LAI further improved the model accuracy in general. The temporal variability of ET makes it
504 challenging to align all of the essential SCOPE parameters in space and time with remote sensing data (Pacheco-Labrador et
505 al., 2020). Given the differences in temporal resolution of the model inputs and ET seasonality (daily and yearly), the validation
506 should not only focus on the general accuracy but also assess the residuals across time and space to evaluate the impact of each
507 parameter in the model performance.

508 **4.3 Model comparison and generalisation**

509 The advantage of a process-based model (i.e. fully deterministic) over an empirical model is that training is not required, which
510 increases the chances of generalising the model to other locations. Our approach can be applied to estimate ET at any location
511 in the city or time aggregation (ranging from hourly to annually). The network of DWD stations could be used to create
512 spatiotemporal raster layers with the primary inputs of atmospheric conditions required to model ET using the grid resolution
513 of the land surface data. Combining high temporal resolution raster data of atmospheric conditions and land cover surface data
514 with high spatial resolution can make it feasible to produce accurate ET maps for entire metropolitan regions. We demonstrate
515 that one meteorological station is enough to provide input variables to characterise the atmospheric conditions for different
516 locations in a large city such as Berlin. For instance, the incoming solar radiation inputs (shortwave and longwave) used in
517 this study were provided by a DWD station located in another town (Potsdam) more than 20 km from both sites. A high spatial
518 resolution is not as crucial to represent the atmospheric conditions as a high temporal resolution (e.g. hourly). However, this
519 approach requires adequate spatial resolution of the vegetation fraction to apply the correction for urban environments.

520 Our approach requires fewer and freely available model inputs, demanding less calibration and computational cost than
521 hydrological and urban models that provide ET or LE as output. For instance, SUEWS models have many non-ordinary inputs
522 that are difficult to supply in a high temporal and spatial resolution (Järvi et al., 2011). Several inputs are described as important
523 in the model, including the fraction of irrigated surface area, soil fraction without rocks and maximum soil storage capacity.
524 Rafael et al. (2020) state that the availability of measured data is a limitation for applications. UT&C models require even
525 more complex parameters, including the wall's distance to the tree trunk (m), albedo and emissivity of walls, the thickness of
526 walls and roofs, and volumetric heat capacity of impervious surfaces, roofs and walls. These variables are possible to estimate
527 for experimental models at a reduced scale but unreasonable to be applied in real-life cases, especially when aiming to map
528 ET at a high spatial resolution for an entire city. While the SCOPE model includes more than 60 inputs, our study shows that
529 calibrating no more than ten inputs was enough to have relatively high accuracy for ET/LE predictions. The remaining
530 parameters were kept constant by default. There are infinite variables and interactions that a model can explore, but a
531 transferable model (empirical or physical-based) requires a source of parsimony.

532 Despite our approach using a simplifying assumption and few required inputs, the prediction accuracy (precision and bias) is
533 compatible with the state-of-the-art urban ET models while potentially more transferable. The estimations of LE may be critical
534 output in most urban models, often showing a low accuracy, especially in dense urban areas. Rafael et al. (2020) applied the
535 SUEWS model in two locations in Portugal, concluding that the performance of LE predictions in suburban areas was far
536 better than the denser urban site (correlation 0.61 and 0.13, respectively). The statement is consistent with previous studies
537 using two areas with different levels of urbanisation, conducted in the surroundings of London (R^2 0.72 and 0.25) and Helsinki
538 (correlation 0.79 and 0.44) (Karsisto et al., 2016; Ward et al., 2016). Although the UT&C model is a very sophisticated and
539 detailed urban model (i.e. urban canyon design), the accuracy is similar to the SUEWS models. The R^2 reported for the three
540 locations (Singapore, Melbourne and Phoenix) range from 0.50 to 0.62 (Meili et al., 2020). However, given that the model
541 was developed and calibrated for these sites, the accuracy may be lower when transferred to a different location or period. Our
542 modelling approach also presents better accuracy for the suburban site ROTH (R^2 0.82) than the build-up area TUCC (R^2 0.47),
543 similar to the SUEWS models. In general, the accuracy of the dense urban sites is lower than more vegetated areas, independent
544 of the model approach. However, a specialised urban model should perform optimally in denser build-up areas as they were
545 designed for such environments.

546 Our study opted to use a simplifying assumption that (dry) impervious surfaces do not evaporate, similarly to other models.
547 Ward et al. (2016) suggest that future model development should allow some evaporation from paved and built-up surfaces
548 other than evaporation of intercepted water. Therefore, the assumption of urban models such as SUEWS is similar to our
549 simplification, which considers that completely impervious surfaces have no ET using the correction factor.

550 We also compared our approach with the hydrological water balance model (ABIMO 3.2), which models and maps evaporation
551 from precipitation for Berlin available in the study "Surface runoff, percolation, total runoff and evaporation from
552 precipitation" (Senate Department for Urban Planning and the Environment, 2019). This model requires approximately twenty-
553 five data inputs for almost 25,000 single sections of the city (blocks, streets and other features), providing a detailed spatial
554 resolution but only an annual temporal resolution which is not updated every year. It reports that around 60 % of Berlin's
555 precipitation evaporates and varies from less than 50 mm/year to more than 400 mm/year according to the land surface and
556 water systems available in the region. Compared with the 2013 edition, evaporation estimated by the ABIMO model has
557 decreased due to the increase of impervious surfaces and the expansion of drainage systems. For the block where the two EC
558 towers are installed, the evaporation from precipitation was reported as 344 mm/year at ROTH and 196 mm/year at the TUCC
559 site. When considering the average footprint of each tower, the annual values of the Berlin Environmental Atlas reduce to 266
560 mm at ROTH and 165 mm at TUCC. Our approach estimated 330 mm and 151 mm, respectively, while the EC observations
561 (gap-filled with MDS) were 336 mm and 188 mm. Our study arrives at similar annual values of ET using a much simpler
562 approach while providing accurate ET estimates at an hourly scale that can better support actions to mitigate the UHI effect.
563 Again, the higher differences are observed at the TUCC site, confirming that the intercepted precipitation on impervious
564 surfaces may cause underestimation in this location.

565 The accuracy (i.e. bias) varied differently based on the season. In general, our models underestimate ET in wintertime.
566 Modelling SCOPE separately for each season may improve the accuracy as aerodynamic, photosynthetic, soil, and canopy
567 constants could be better specified for these periods. Given that most of the applications to model ET are constrained to the
568 growing season, constants and default parameters are likely to be optimised for these conditions (Ward et al., 2016). Tuning
569 or measuring most of the input parameters to match the reality of the specific urban environment under consideration can
570 further improve the model accuracy. SCOPE has more than sixty model inputs, allowing for greater model customisation to
571 the local environment than presented in this study. However, the objective of this study was to demonstrate the potential of
572 our approach for estimating hourly ET with open data rather than to provide a final model for Berlin. Thus, most of the
573 parameters were kept constant using default model values. Process-based models (SCOPE or hydrological) provide the
574 opportunity to perform sensitivity analysis and simulate scenarios to understand the impact of underlying drivers of ET on
575 accuracy. The latent heat flux from SCOPE can be separated into soil LE and canopy LE, which can be used to improve the
576 correction factor as transpiration and evaporation may differ across seasons and land surfaces. By separating soil LE, the
577 influence of different levels of imperviousness on ET could be better investigated.
578 Applications providing accurate ET maps can range from controlling irrigation for managing green spaces in cities to planning
579 more sustainable urban environments. Such maps could also support local governments in mitigating UHI effects, reducing
580 health risks during extreme summer temperatures. Smart and green city initiatives could utilise dynamic ET maps to monitor
581 the impact of climate change and identify solutions to improve the quality of life in cities worldwide. A better understanding
582 and management of the water cycle (green, blue and grey) will be vital for human well-being in the near future.

583 5. Conclusion

584 This study has proposed a novel approach to estimate hourly evapotranspiration (ET) in urban environments using a process-
585 based model and freely available meteorological and remote sensing data. Therefore, this modelling approach can predict ET
586 in an entire city in different spatial and temporal resolutions, paving the way for mapping urban ET systematically without
587 highly specialised and costly EC tower equipment. Although the SCOPE model was successfully applied to predict ET in
588 previous studies, this is the first time that SCOPE has been applied in an urban environment. Most process-based model
589 approaches to estimating ET, including SCOPE, are designed for homogeneous vegetated landscapes, resulting in the
590 overestimation of ET in urban areas. However, we developed a correction factor for urban environments using vegetation
591 fraction derived from remote sensing data that has proved to reduce model bias and improve global accuracy. The solution
592 combines high temporal resolution data of atmospheric conditions from meteorological stations and high spatial resolution
593 data of land surface derived from remote sensing. We demonstrate that a single meteorological station is enough to provide
594 model input to characterise the atmospheric conditions for different locations in a city, which increases the potential to
595 generalise the approach to produce ET maps for other urban regions. The model performance decreases at nighttime, winter
596 and in the presence of wet surfaces as interception loss is not considered. However, these conditions are not important for

597 adapting to droughts and mitigating the urban heat island (UHI). Therefore, our approach is well-suited to produce ET maps
598 that are highly relevant to urban planning and climate change mitigation.

599 **Code and data availability**

600 The SCOPE documentation and codes are freely available (<https://scope-model.readthedocs.io/en/latest/mSCOPE.html> and
601 <https://github.com/peiqiyang/mSCOPE>). The data used are available from the author upon request.

602 **Author contributions**

603 ADR and BK were responsible for the overall research goals and aims. ADR was responsible to prepared the manuscript draft.
604 SV and ADR co-worked in the measured data pre-processing and footprint modelling. ADR was responsible for the modelling
605 and results and CT as curated and specialist in SCOPE model. MF and BK contribute to the remote sensing inputs and model
606 evaluation. All authors contributed to discussion of results and the evolution of the written manuscript.

607 **Competing interests**

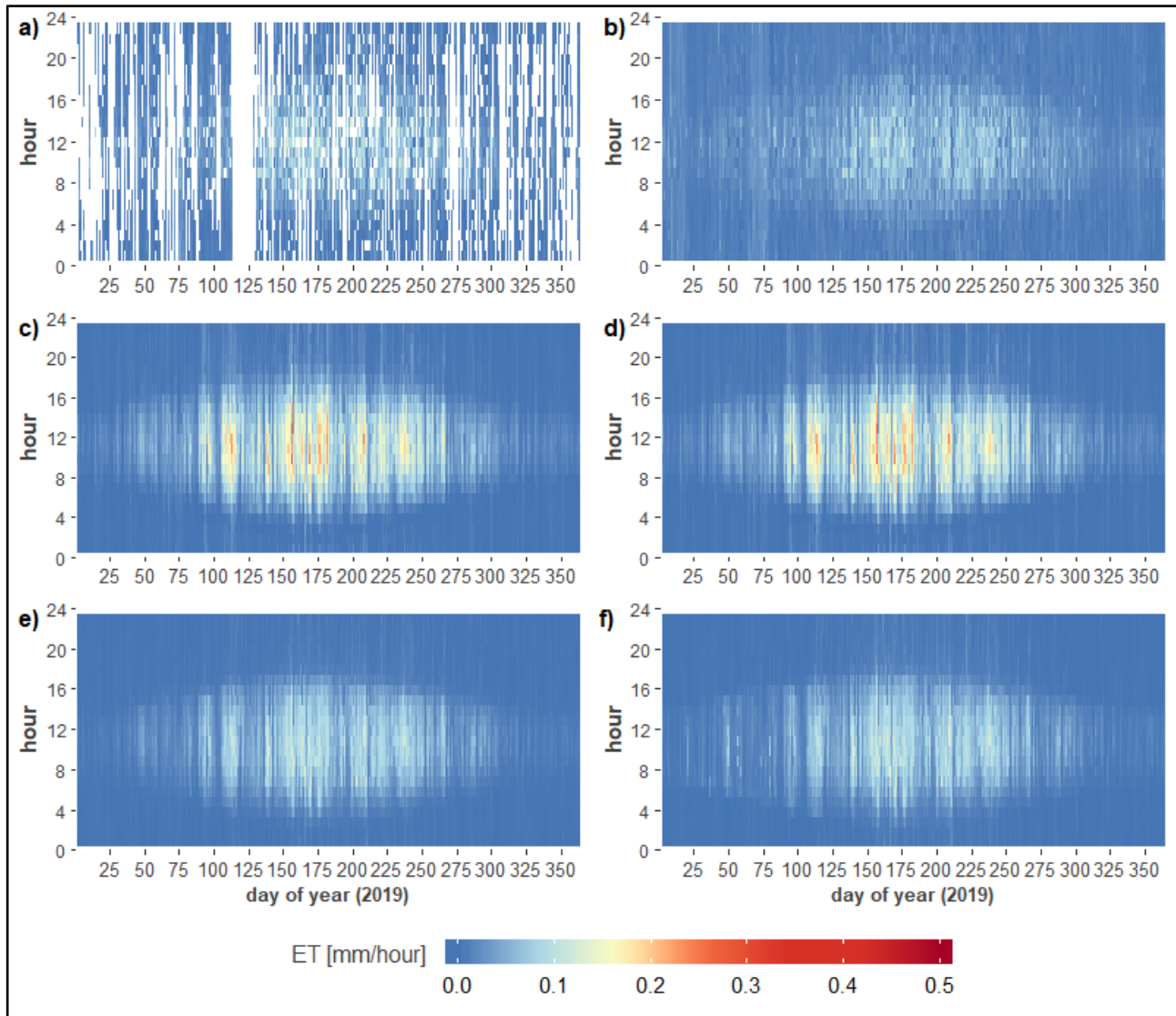
608 The authors declare that they have no conflict of interest

609 **Acknowledgements**

610 This work was supported by the German Research Foundation (DFG) within the Research Training Group 'Urban Water
611 Interfaces' (GRK 2032-2). The German Federal Ministry of Education and Research (BMBF) funded instrumentation of the
612 Urban Climate Observatory (UCO) Berlin under grant 01LP1602 within the framework of Research for Sustainable
613 Development (FONA; 635 www.fona.de). The authors would like to thank the DWD, the Chair of Climatology at the
614 Technische Universität Berlin, the European Commission, and the Berlin Senate Department for Urban Development and
615 Housing for providing data used in this paper. We would additionally like to thank Fred Meier for pre-processing and providing
616 the eddy covariance data and Justus Quanz for providing R code to optimise footprint modelling.

617

618



620

621 **Figure A1.** ET by day of the year and hours of the day for the TUCC site. Observed ET after cleaning (a), observed ET gap-filled with MDS
 622 (b), Penman-Monteith ET₀ (c), predicted ET with SCOPE_ET₀ model (d), predicted ET with SCOPE_DWD model (e), and predicted ET
 623 with SCOPE_RS model (f).

624 **References**

- 625 Allen, R. G., Pereira, L. S., Raes, D. and Smith, M.: Crop evapotranspiration: Guidelines for computing crop requirements.
 626 FAO Irrigation and drainage paper 56., 1998.
 627 Allen, R. G., Walter, I. A., Elliott, R. L., Howell, T. A., Itenfisu, D., Jensen, M. E. and Snyder, R. L.: The ASCE Standardized

628 Reference Evapotranspiration Equation, American Society of Civil Engineers., 2005.

629 Bauer-Marschallinger, B. and Paulik, C.: Copernicus Global Land Operations "Vegetation and Energy". Validation Report
630 (QAR). SWI1km-V1_I1.11, 2019.

631 Bayat, B., van der Tol, C. and Verhoef, W.: Integrating satellite optical and thermal infrared observations for improving daily
632 ecosystem functioning estimations during a drought episode, *Remote Sens. Environ.*, 209(January), 375–394,
633 doi:10.1016/j.rse.2018.02.027, 2018.

634 Devia, G. K., Ganasri, B. P. and Dwarakish, G. S.: A Review on Hydrological Models, *Aquat. Procedia*, 4(Icwrcoe), 1001–
635 1007, doi:10.1016/j.aqpro.2015.02.126, 2015.

636 Dwarakish, G. S., Ganasri, B. P. and De Stefano, L.: Impact of land use change on hydrological systems: A review of current
637 modeling approaches, *Cogent Geosci.*, 1(1), 1115691, doi:10.1080/23312041.2015.1115691, 2015.

638 DWD: DWD Climate Data Center (CDC), [online] Available from: http://ftp-cdc.dwd.de/climate_environment/CDC/, 2020.

639 Falge, E., Baldocchi, D., Olson, R., Anthoni, P., Aubinet, M., Bernhofer, C., Burba, G., Ceulemans, R., Clement, R., Dolman,
640 H., Granier, A., Gross, P., Grünwald, T., Hollinger, D., Jensen, N. O., Katul, G., Keronen, P., Kowalski, A., Lai, C. T., Law,
641 B. E., Meyers, T., Moncrieff, J., Moors, E., Munger, J. W., Pilegaard, K., Rannik, Ü., Rebmann, C., Suyker, A., Tenhunen, J.,
642 Tu, K., Verma, S., Vesala, T., Wilson, K. and Wofsy, S.: Gap filling strategies for defensible annual sums of net ecosystem
643 exchange, *Agric. For. Meteorol.*, 107(1), 43–69, doi:10.1016/S0168-1923(00)00225-2, 2001.

644 Feigenwinter, C., Vogt, R. and Christen, A.: Eddy Covariance, *Eddy Covariance*, 377–397, doi:10.1007/978-94-007-2351-1,
645 2012.

646 Feigenwinter, C., Vogt, R., Parlow, E., Lindberg, F., Marconcini, M., Frate, F. Del and Chrysoulakis, N.: Spatial Distribution
647 of Sensible and Latent Heat Flux in the City of Basel (Switzerland), *IEEE J. Sel. Top. Appl. Earth Obs. Remote Sens.*, 11(8),
648 2717–2723, doi:10.1109/JSTARS.2018.2807815, 2018.

649 Foken, T.: The energy balance closure problem: An overview, *Ecol. Appl.*, 18(6), 1351–1367, doi:10.1890/06-0922.1, 2008.

650 Foltýnová, L., Fischer, M. and McGloin, R. P.: Recommendations for gap-filling eddy covariance latent heat flux
651 measurements using marginal distribution sampling, *Theor. Appl. Climatol.*, 139(1–2), 677–688, doi:10.1007/s00704-019-
652 02975-w, 2020.

653 Gillefalk, M., Tetzlaff, D., Hinkelmann, R., Kuhlemann, L., Meier, F., Maneta, M. P. and Soulsby, C.: Quantifying the effects
654 of urban green space on water partitioning and ages using an isotope-based ecohydrological model, , (January), 1–27, 2021.

655 Hörnschemeyer, B., Henrichs, M. and Uhl, M.: Swmm-urbaneva: A model for the evapotranspiration of urban vegetation,
656 *Water (Switzerland)*, 13(2), doi:10.3390/w13020243, 2021.

657 Järvi, L., Grimmond, C. S. B. and Christen, A.: The Surface Urban Energy and Water Balance Scheme (SUEWS): Evaluation
658 in Los Angeles and Vancouver, *J. Hydrol.*, 411(3–4), 219–237, doi:10.1016/j.jhydrol.2011.10.001, 2011.

659 Karsisto, P., Fortelius, C., Demuzere, M., Grimmond, C. S. B., Oleson, K. W., Kouznetsov, R., Masson, V. and Järvi, L.:
660 Seasonal surface urban energy balance and wintertime stability simulated using three land-surface models in the high-latitude
661 city Helsinki, *Q. J. R. Meteorol. Soc.*, 142(694), 401–417, doi:10.1002/qj.2659, 2016.

662 Kent, C. W., Grimmond, S. and Gatey, D.: Aerodynamic roughness parameters in cities: Inclusion of vegetation, *J. Wind Eng.*
663 *Ind. Aerodyn.*, 169, 168–176, doi:10.1016/j.jweia.2017.07.016, 2017.

664 Kljun, N., Rotach, M. W. and Schmid, H. P.: A three-dimensional backward lagrangian footprint, *Boundary-Layer Meteorol.*,
665 103, 205–226, 2002.

666 Kljun, N., Calanca, P., Rotach, M. W. and Schmid, H. P.: A simple two-dimensional parameterisation for Flux Footprint
667 Prediction (FFP), *Geosci. Model Dev.*, 8(11), 3695–3713, doi:10.5194/gmd-8-3695-2015, 2015.

668 Knauer, J., El-Madany, T. S., Zaehle, S. and Migliavacca, M.: Bigleaf - An R package for the calculation of physical and
669 physiological ecosystem properties from eddy covariance data, *PLoS One*, 13(8), e0201114,
670 doi:10.1371/journal.pone.0201114, 2018.

671 Kormann, R. and Meixner, F. X.: An analytical footprint model for non-neutral stratification, *Boundary-Layer Meteorol.*,
672 99(2), 207–224, doi:10.1023/A:1018991015119, 2001.

673 Kotthaus, S. and Grimmond, C. S. B.: Identification of Micro-scale Anthropogenic CO₂, heat and moisture sources -
674 Processing eddy covariance fluxes for a dense urban environment, *Atmos. Environ.*, 57, 301–316,
675 doi:10.1016/j.atmosenv.2012.04.024, 2012.

676 Kotthaus, S. and Grimmond, C. S. B.: Energy exchange in a dense urban environment - Part II: Impact of spatial heterogeneity
677 of the surface, *Urban Clim.*, 10(P2), 281–307, doi:10.1016/j.uclim.2013.10.001, 2014.

678 Kovats, R. S. and Hajat, S.: Heat stress and public health: A critical review, *Annu. Rev. Public Health*, 29, 41–55,
679 doi:10.1146/annurev.publhealth.29.020907.090843, 2008.

680 Kracher, D., Mengelkamp, H. T. and Foken, T.: The residual of the energy balance closure and its influence on the results of
681 three SVAT models, *Meteorol. Zeitschrift*, 18(6), 647–661, doi:10.1127/0941-2948/2009/0412, 2009.

682 Liang, S. and Wang, J., Eds.: Chapter 17 - Terrestrial evapotranspiration, in *Advanced Remote Sensing (Second Edition)*, pp.
683 649–684, Academic Press., 2020.

684 Maronga, B., Gryschka, M., Heinze, R., Hoffmann, F., Kanani-Sühring, F., Keck, M., Ketelsen, K., Letzel, M. O., Sühring,
685 M. and Raasch, S.: The Parallelized Large-Eddy Simulation Model (PALM) version 4.0 for atmospheric and oceanic flows:
686 Model formulation, recent developments, and future perspectives, *Geosci. Model Dev.*, 8(8), 2515–2551, doi:10.5194/gmd-8-
687 2515-2015, 2015.

688 Martens, B., Miralles, D. G., Lievens, H., Van Der Schalie, R., De Jeu, R. A. M., Fernández-Prieto, D., Beck, H. E., Dorigo,
689 W. A. and Verhoest, N. E. C.: GLEAM v3: Satellite-based land evaporation and root-zone soil moisture, *Geosci. Model Dev.*,
690 10(5), 1903–1925, doi:10.5194/gmd-10-1903-2017, 2017.

691 Meili, N., Manoli, G., Burlando, P., Bou-Zeid, E., Chow, W. T. L., Coutts, A. M., Daly, E., Nice, K. A., Roth, M., Tapper, N.
692 J., Velasco, E., Vivoni, E. R. and Faticchi, S.: An urban ecohydrological model to quantify the effect of vegetation on urban
693 climate and hydrology (UT&C v1.0), *Geosci. Model Dev.*, 13(1), 335–362, doi:10.5194/gmd-13-335-2020, 2020.

694 Miralles, D. G., Brutsaert, W., Dolman, A. J. and Gash, J. H.: On the Use of the Term “Evapotranspiration,” *Water Resour.*
695 *Res.*, 56(11), doi:10.1029/2020WR028055, 2020.

696 Moncrieff, J. B., Massheder, J. M., Bruin, H. De, Elbers, J., Friborg, T., Heusinkveld, B., Kabat, P., Scott, S., Soegaard, H.
697 and Verhoef, A.: A system to measure surface fluxes of momentum, sensible heat, water vapour and carbon dioxide, *J. Hydrol.*,
698 188–189(1–4), 589–611, doi:10.1016/S0022-1694(96)03194-0, 1997.

699 Nordbo, A., Järvi, L. and Vesala, T.: Revised eddy covariance flux calculation methodologies - effect on urban energy balance,
700 *Tellus, Ser. B Chem. Phys. Meteorol.*, 64(1), doi:10.3402/tellusb.v64i0.18184, 2012.

701 Nouri, H., Beecham, S., Kazemi, F. and Hassanli, A. M.: A review of ET measurement techniques for estimating the water
702 requirements of urban landscape vegetation, *Urban Water J.*, 10(4), 247–259, doi:10.1080/1573062X.2012.726360, 2013.

703 Nouri, H., Beecham, S., Anderson, S., Hassanli, A. M. and Kazemi, F.: Remote sensing techniques for predicting
704 evapotranspiration from mixed vegetated surfaces, *Urban Water J.*, 12(5), 380–393, doi:10.1080/1573062X.2014.900092,
705 2015.

706 Nouri, H., Borujeni, S. C. and Hoekstra, A. Y.: The blue water footprint of urban green spaces: An example for Adelaide,
707 Australia, *Landsc. Urban Plan.*, 190, 103613, doi:10.1016/j.landurbplan.2019.103613, 2019.

708 Olmedo, G. F., Ortega-Farías, S., de la Fuente-Sáiz, D., Fonseca-Luengo, D. and Fuentes-Peñailillo, F.: water: Tools and
709 Functions to Estimate Actual Evapotranspiration Using Land Surface Energy Balance Models in R, *R J.*, 8(2), 352–370,
710 doi:10.32614/rj-2016-051, 2016.

711 Ortega-Farias, S., Olioso, A., Antonioletti, R. and Brisson, N.: Evaluation of the Penman-Monteith model for estimating
712 soybean evapotranspiration, *Irrig. Sci.*, 23(1), 1–9, doi:10.1007/s00271-003-0087-1, 2004.

713 Pacheco-Labrador, J., El-Madany, T., van der Tol, C., Martin, M. P., Gonzalez-Cascon, R., Perez-Priego, O., Guan, J., Moreno,
714 G., Carrara, A., Reichstein, M. and Migliavacca, M.: senSCOPE: Modeling radiative transfer and biochemical processes in
715 mixed canopies combining green and senescent leaves with SCOPE, *bioRxiv*, doi:10.1101/2020.02.05.935064, 2020.

716 Petropoulos, G., Carlson, T. N. and Wooster, M. J.: An overview of the use of the SimSphere Soil Vegetation Atmosphere
717 Transfer (SVAT) model for the study of land-atmosphere interactions, *Sensors*, 9(6), 4286–4308, doi:10.3390/s90604286,
718 2009.

719 Quanz, J. A.: Impact of spatial heterogeneity on energy exchange in an urban environment in Berlin, Germany, 2018.

720 R Core Team: R: A Language and Environment for Statistical Computing, [online] Available from: <https://www.r-project.org/>,
721 2020.

722 Rafael, S., Rodrigues, V., Fernandes, A. P., Augusto, B., Borrego, C. and Lopes, M.: Evaluation of urban surface
723 parameterizations in WRF model using energy fluxes measurements in Portugal, *Urban Clim.*, 28(March), 100465,
724 doi:10.1016/j.uclim.2019.100465, 2019.

725 Rafael, S., Martins, H., Matos, M. J., Cerqueira, M., Pio, C., Lopes, M. and Borrego, C.: Application of SUEWS model forced
726 with WRF: Energy fluxes validation in urban and suburban Portuguese areas, *Urban Clim.*, 33(May), 100662,
727 doi:10.1016/j.uclim.2020.100662, 2020.

728 Ramamurthy, P. and Bou-Zeid, E.: Contribution of impervious surfaces to urban evaporation, *Water Resour. Res.*, 50(4), 2889–
729 2902, doi:10.1002/2013WR013909, 2014.

730 Rocha, A. D., Groen, T. A., Skidmore, A. K., Darvishzadeh, R. and Willemsen, L.: Machine learning using hyperspectral data
731 inaccurately predicts plant traits under spatial dependency, *Remote Sens.*, 10(8), doi:10.3390/rs10081263, 2018.

732 Rocha, A. D., Groen, T. A., Skidmore, A. K. and Willemsen, L.: Role of Sampling Design When Predicting Spatially Dependent
733 Ecological Data With Remote Sensing, *IEEE Trans. Geosci. Remote Sens.*, 1–12, doi:10.1109/TGRS.2020.2989216, 2020.

734 Scherer, D., Fehrenbach, U., Lakes, T., Lauf, S., Meier, F. and Schuster, C.: Quantification of heat-Stress related mortality
735 hazard, vulnerability and risk in Berlin, Germany, *Erde*, 144(3–4), 238–259, doi:10.12854/erde-144-17, 2013.

736 Scherer, D., Ament, F., Emeis, S., Fehrenbach, U., Leitl, B., Scherber, K., Schneider, C. and Vogt, U.: Three-dimensional
737 observation of atmospheric processes in cities, *Meteorol. Zeitschrift*, 28(2), 121–138, doi:10.1127/metz/2019/0911, 2019.

738 Schmid, H. P. and Oke, T. R.: A model to estimate the source area contributing to turbulent exchange in the surface layer over
739 patchy terrain, *Q. J. R. Meteorol. Soc.*, 116(494), 965–988, doi:10.1002/qj.49711649409, 1990.

740 Senate Department for Urban Development and Housing: Berlin Environmental Atlas, Green Volume (Edition 2017).
741 Retrieved from https://www.stadtentwicklung.berlin.de/umwelt/umweltatlas/e_text/ek509.pdf, 2017.

742 Senate Department for Urban Planning and the Environment: Berlin Environmental Atlas, Building and Vegetation Heights
743 (2014 Edition). Retrieved from https://www.stadtentwicklung.berlin.de/umwelt/umweltatlas/e_text/ek610.pdf, 2014.

744 Senate Department for Urban Planning and the Environment: Berlin Environmental Atlas, Surface Runoff, Percolation, Total
745 Runoff and Evaporation from Precipitation (2019 Edition). Retrieved from
746 https://www.berlin.de/umweltatlas/_assets/wasser/wasserhaushalt/en-texte/ekd213.pdf, 2019.

747 Timmermans, J., Su, Z., van der Tol, C., Verhoef, A. and Verhoef, W.: Quantifying the uncertainty in estimates of surface-
748 atmosphere fluxes through joint evaluation of the SEBS and SCOPE models, *Hydrol. Earth Syst. Sci.*, 17(4), 1561–1573,
749 doi:10.5194/hess-17-1561-2013, 2013.

750 van der Tol, C. and Norberto, G.: Guidelines for Remote Sensing of Evapotranspiration, *Evapotranspiration - Remote Sens.*
751 *Model.*, doi:10.5772/18582, 2012.

752 van der Tol, C., Verhoef, W., Timmermans, J., Verhoef, A. and Su, Z.: An integrated model of soil-canopy spectral radiances,
753 photosynthesis, fluorescence, temperature and energy balance, *Biogeosciences*, 6(12), 3109–3129, doi:10.5194/bg-6-3109-
754 2009, 2009.

755 Vickers, D. and Mahrt, L.: Quality control and flux sampling problems for tower and aircraft data, *J. Atmos. Ocean. Technol.*,
756 14(3), 512–526, doi:10.1175/1520-0426(1997)014<0512:QCAFSP>2.0.CO;2, 1997.

757 Vitale, D., Fratini, G., Bilancia, M., Nicolini, G., Sabbatini, S. and Papale, D.: A robust data cleaning procedure for eddy
758 covariance flux measurements, *Biogeosciences*, 17(6), 1367–1391, doi:10.5194/bg-17-1367-2020, 2020.

759 Vulova, S., Meier, F., Duarte, A., Quanz, J., Nouri, H. and Kleinschmit, B.: Science of the Total Environment Modeling urban
760 evapotranspiration using remote sensing , flux footprints , and artificial intelligence , 786,
761 doi:10.1016/j.scitotenv.2021.147293, 2021.

762 Wang, Y., Zhang, Y., Ding, N., Qin, K. and Yang, X.: Simulating the impact of urban surface evapotranspiration on the urban
763 heat island effect using the modified RS-PM model: A case study of Xuzhou, China, *Remote Sens.*, 12(3),

764 doi:10.3390/rs12030578, 2020.

765 Ward, H. C. and Grimmond, C. S. B.: Assessing the impact of changes in surface cover, human behaviour and climate on
766 energy partitioning across Greater London, *Landsc. Urban Plan.*, 165(February), 142–161,
767 doi:10.1016/j.landurbplan.2017.04.001, 2017.

768 Ward, H. C., Evans, J. G. and Grimmond, C. S. B.: Multi-season eddy covariance observations of energy, water and carbon
769 fluxes over a suburban area in Swindon, UK, *Atmos. Chem. Phys.*, 13(9), 4645–4666, doi:10.5194/acp-13-4645-2013, 2013a.

770 Ward, H. C., Evans, J. G. and Grimmond, C. S. B. B.: Multi-season eddy covariance observations of energy, water and carbon
771 fluxes over a suburban area in Swindon, UK, *Atmos. Chem. Phys.*, 13(9), 4645–4666, doi:10.5194/acp-13-4645-2013, 2013b.

772 Ward, H. C., Kotthaus, S., Järvi, L. and Grimmond, C. S. B.: Surface Urban Energy and Water Balance Scheme (SUEWS):
773 Development and evaluation at two UK sites, *Urban Clim.*, 18, 1–32, doi:10.1016/j.uclim.2016.05.001, 2016.

774 Webb, E. K., Pearman, G. I. and Leuning, R.: Correction of flux measurements for density effects due to heat and water vapour
775 transfer, *Q. J. R. Meteorol. Soc.*, 106(447), 85–100, doi:10.1002/qj.49710644707, 1980.

776 Westerhoff, R. S.: Using uncertainty of Penman and Penman-Monteith methods in combined satellite and ground-based
777 evapotranspiration estimates, *Remote Sens. Environ.*, 169, 102–112, doi:10.1016/j.rse.2015.07.021, 2015.

778 Wickham, H.: *ggplot2*, Springer International Publishing, Cham., 2016.

779 Wouters, H., Demuzere, M., Ridder, K. De and Van Lipzig, N. P. M.: The impact of impervious water-storage parametrization
780 on urban climate modelling, *Urban Clim.*, 11(C), 24–50, doi:10.1016/j.uclim.2014.11.005, 2015.

781 Wutzler, T., Lucas-Moffat, A., Migliavacca, M., Knauer, J., Sickel, K., Šigut, L., Menzer, O. and Reichstein, M.: Basic and
782 extensible post-processing of eddy covariance flux data with REddyProc, *Biogeosciences Discuss.*, 1–39, doi:10.5194/bg-
783 2018-56, 2018.

784 Xenakis, G.: FREddyPro: Post-Processing EddyPro Full Output File (R package version 1.0), [online] Available from:
785 <https://cran.r-project.org/package=FREddyPro>, 2016.

786 Yang, P., Prikaziuk, E., Verhoef, W. and Tol, C. Van Der: SCOPE 2 . 0 : A model to simulate vegetated land surface fluxes
787 and satellite signals, , (October), 1–26, doi:https://doi.org/10.5194/gmd-2020-251, 2020.

788 Zhao, L., Xia, J., Xu, C. yu, Wang, Z., Sobkowiak, L. and Long, C.: Evapotranspiration estimation methods in hydrological
789 models, *J. Geogr. Sci.*, 23(2), 359–369, doi:10.1007/s11442-013-1015-9, 2013.

790 Zheng, Q., Hao, L., Huang, X., Sun, L. and Sun, G.: Effects of urbanization on watershed evapotranspiration and its
791 components in southern China, *Water (Switzerland)*, 12(3), doi:10.3390/w12030645, 2020.

792